Constraints on large-x parton distributions from new weak boson production and deep-inelastic scattering data

A. Accardi,[1,2] L. T. Brady,[2,3] W. Melnitchouk,[2] J. F. Owens,[4] and N. Sato[2]

[1]*Hampton University, Hampton, Virginia 23668, USA*
[2]*Jefferson Lab, Newport News, Virginia 23606, USA*
[3]*University of California, Santa Barbara, California 93106, USA*
[4]*Florida State University, Tallahassee, Florida 32306, USA*
(Received 15 February 2016; published 20 June 2016)

We present a new set of leading-twist parton distribution functions, referred to as "CJ15," which take advantage of developments in the theoretical treatment of nuclear corrections as well as new data. The analysis includes, for the first time, data on the free neutron structure function from Jefferson Lab and new high-precision charged lepton and W-boson asymmetry data from Fermilab. These significantly reduce the uncertainty on the d/u ratio at large values of x and provide new insights into the partonic structure of bound nucleons.

I. INTRODUCTION

Tremendous advances have been made over the past decade in our knowledge of the quark and gluon (or parton) substructure of the nucleon, with the availability of new high-energy scattering data from various accelerator facilities worldwide [1–3]. Results from the final analysis of data from the ep collider HERA have allowed a detailed mapping of the partonic landscape at small values of the nucleon's parton momentum fraction x [4]. Data from high-energy $p\bar{p}$ scattering at the Tevatron on weak boson and jet production have provided a wealth of complementary information on the nucleon's flavor structure. At lower energies, precision structure function measurements at the high-luminosity CEBAF accelerator at Jefferson Lab have enabled a detailed investigation of nucleon structure at large values of x [5]. More recently, fascinating glimpses into the role played by sea quarks and gluons in the proton have been seen in various channels in pp collisions at the LHC.

To analyze the vast amounts of data from the various facilities, concerted efforts are being made to systematically extract information about the nucleon's quark and gluon structure in the form of parton distribution functions (PDFs) [6–14]. While much of the effort has in the past been directed at the small-x frontier made accessible through the highest-energy colliders, relatively less attention has been focused on the region of large momentum fractions, where nonperturbative QCD effects generally play a more important role.

The CTEQ-Jefferson Lab (CJ) Collaboration [15] has performed a series of global PDF analyses [12–14] with the aim of maximally utilizing data at the highest-x values amenable to perturbative QCD treatment. The additional complications of working with data down to relatively low values of four-momentum transfer Q^2 ($Q^2 \gtrsim 1$–2 GeV^2)

and invariant final state masses W^2 ($W^2 \gtrsim 4$ GeV^2) have been met with developments in the theoretical description of various effects which come into prominence at such kinematics. The importance of $1/Q^2$ power corrections, arising from target mass and higher-twist effects, has been emphasized [12,13] particularly in the analysis of fixed-target deep-inelastic scattering (DIS) data, which found leading-twist PDFs to be stable down to low-Q^2 values with the inclusion of both of these effects.

Moreover, since the CJ analyses typically fit both proton and deuterium data, the description of the latter requires careful treatment of nuclear corrections at large values of x, at all Q^2 scales. The d-quark PDF is especially sensitive to the deuterium corrections for $x \gtrsim 0.5$, and historically has suffered from large uncertainties due to the model dependence of the nuclear effects [16]. To adequately allow for the full range of nuclear model uncertainties, the CJ12 analysis [14] produced three sets of PDFs corresponding to different strengths (minimum, medium and maximum) of the nuclear effects, which served to provide a more realistic estimate of the d-quark PDF uncertainty compared with previous fits.

In this analysis, which we refer to as "CJ15," we examine the impact of new large rapidity charged lepton and W-boson asymmetry data from the Tevatron [17–19] on the determination of next-to-leading-order (NLO) PDFs and their errors, particularly at large values of x. We also include for the first time new Jefferson Lab data on the free neutron structure function obtained from backward spectator proton tagging in semi-inclusive DIS [20,21], which do not suffer from the same uncertainties that have afflicted previous neutron extractions. We present a more complete treatment of the nuclear corrections in deuterium, examining a range of high-precision deuteron wave functions and several models for the nucleon off-shell corrections. In contrast to our earlier fits [12–14], which relied on

physically motivated models for the off-shell effects, the precision of the new data allows us to perform a purely phenomenological fit, with the off-shell parameters determined directly from the data. Other improvements in the CJ15 analysis include a more robust parametrization of the $\bar{d}/\bar{u}$ asymmetry, which accommodates different asymptotic behaviors as $x \to 1$, and the implementation of the S-ACOT scheme [22] for heavy quarks.

In Sec. II, we review the theoretical formalism underpinning our global analysis, including the choice of parametrization for the various PDFs. We discuss the treatment of mass thresholds, and the application of finite-Q^2 corrections from target mass and higher-twist effects that are necessary to describe the low-Q^2, large-x data. A detailed investigation of nuclear corrections in the deuteron follows, in which we outline several models and parametrizations of nucleon off-shell corrections, which represent the main uncertainty in the computation of the nuclear effects.

In Sec. III, a summary of the data sets used in this analysis is given, and the results of the fits are presented in Sec. IV. Here we compare the CJ15 PDFs with other modern parametrizations, as well as with selected observables. In addition to the NLO analysis, we also perform a leading-order (LO) fit, which is useful for certain applications, such as Monte Carlo generators or for estimating cross sections and event rates for new experiments. Our central results deal with the role played by the nuclear corrections and their uncertainties in the global analysis, and how these can be reduced by exploiting the interplay of different observables sensitive to the d-quark PDF. We discuss the consequences of the new analysis for the shape of the deuteron to isoscalar nucleon structure function ratio, and the closely related question of the behavior of the d/u PDF ratio at large x. Finally, in Sec. V we summarize our results and discuss possible future improvements in PDF determination that are expected to come with new data from collider and fixed-target experiments.

II. THEORETICAL FOUNDATIONS

In this section, we present the theoretical framework on which the CJ15 PDF analysis is based. We begin with a discussion of the parametrizations chosen for the various flavor PDFs, noting the particular forms used here for the d/u and $\bar{d}/\bar{u}$ ratios compared with earlier work. We then describe our treatment of heavy quarks, and the implementation of finite-Q^2 corrections. A detailed discussion of the nuclear corrections in the deuteron follows, where we review previous attempts to account for nucleon off-shell effects and describe the approach taken in this analysis.

A. PDF parametrizations

For the parametrization of the PDFs at the input scale Q_0^2, chosen here to be the mass of the charm quark, $Q_0^2 = m_c^2$, a standard five-parameter form is adopted for most parton species f,

$$xf(x, Q_0^2) = a_0 x^{a_1}(1-x)^{a_2}(1 + a_3\sqrt{x} + a_4 x). \quad (1)$$

This form applies to the valence $u_v = u - \bar{u}$ and $d_v = d - \bar{d}$ distributions, the light antiquark sea $\bar{u} + \bar{d}$, and the gluon distribution g. The charm quark is considered to be radiatively generated from the gluons. To allow greater flexibility for the valence d_v PDF in the large-x region, we add in a small admixture of the valence u-quark PDF,

$$d_v \to a_0^{d_v}\left(\frac{d_v}{a_0^{d_v}} + bx^c u_v\right), \quad (2)$$

with b and c as two additional parameters. The result of this modification is that the ratio $d_v/u_v \to a_0^{d_v} b$ as $x \to 1$, provided that $a_2^{d_v} > a_2^{u_v}$, which is usually the case. This form avoids potentially large biases on the d-quark PDF central value [13], as well as on its PDF error estimate [23], as we discuss in detail in Sec. IV. A finite, nonzero value of the d_v/u_v ratio is also expected in several nonperturbative models of hadron structure [16,24–28]. The normalization parameters a_0 for the u_v and d_v distributions are fixed by the appropriate valence quark number sum rules, while a_0^g is fixed by the momentum sum rule.

In the CJ12 PDF sets the combinations $\bar{d} \pm \bar{u}$ were parametrized separately. In that analysis it was found to be difficult to control the size of the $\bar{d}$ distribution relative to the $\bar{u}$ at values of x above about 0.3, since there were essentially no constraints on the sea quarks. Consequently some fits generated $\bar{d}$ PDFs that became negative in this region. While this had little effect on the NLO fits since the terms were very small there, it was nonetheless unsatisfactory when one considered LO fits where the PDFs are expected to be positive. In the present analysis we therefore parametrize directly the ratio $\bar{d}/\bar{u}$ instead of the difference $\bar{d} - \bar{u}$. For the functional form of $\bar{d}/\bar{u}$ at the input scale Q_0^2, we choose

$$\frac{\bar{d}}{\bar{u}} = a_0 x^{a_1}(1-x)^{a_2} + 1 + a_3 x(1-x)^{a_4}, \quad (3)$$

which ensures that in the limit $x \to 1$ one has $\bar{d}/\bar{u} \to 1$. This is actually a theoretical prejudice since the sea quark PDFs are fed by Q^2 evolution which, in the absence of isospin symmetry violating effects, generates equal $\bar{d}$ and $\bar{u}$ contributions.

Since the existing data are not able to reliably determine the large-x behavior of the ratio, we have also performed alternative fits using $\bar{d}/\bar{u} = a_0 x^{a_1}(1-x)^{a_2} + (1 + a_3 x)(1-x)^{a_4}$, which vanishes in the $x \to 1$ limit. Data from the E866 dilepton production experiment [29,30] currently provide the strongest constraints on the $\bar{d}/\bar{u}$ ratio

and show a decrease below unity in the region $x \gtrsim 0.3$, albeit with large errors. It was found that either parametrization could achieve excellent fits to the data included in the global analysis. In the central fits presented here, we choose the parametrization in Eq. (3). In the near future, the SeaQuest experiment (E906) [31] at Fermilab is expected to yield data with greater statistical precision that will constrain the $\bar{d}/\bar{u}$ ratio to larger x values and so answer the question as to which parametrization is more suitable. Data on Drell-Yan and W-boson production in pp collisions at the LHC should also provide important constraints on the behavior of $\bar{d}/\bar{u}$ outside of currently accessible regions of x.

For the strange quark distribution, the strongest constraints have traditionally come from charm meson production in neutrino DIS from nuclei. In keeping with the approach adopted in our previous analyses [12–14], we do not include neutrino scattering data in the current fit because of uncertainties in relating structure functions of heavy nuclei to those of free nucleons. Moreover, a proper treatment of dimuon production on nuclear targets requires inclusion of initial state as well as final state nuclear effects [32,33]. The former are relatively well understood and accounted for by using nuclear PDFs [34–36]. The latter, however, include effects such as the scattered charm quark energy loss while traversing the target nucleus or D meson–nucleon interactions for mesons hadronizing within the nucleus, which are much less known. These effects have often been underestimated theoretically in the analysis of heavy-ion reactions and are essentially unknown experimentally in nuclear DIS, constituting a potentially large source of systematic uncertainty. Consequently, we follow our previous strategy in assuming flavor independence of the shape of the sea quark PDFs, with a fixed ratio

$$\kappa = \frac{s + \bar{s}}{\bar{u} + \bar{d}}. \tag{4}$$

We further make the usual assumption that $\bar{s} = s$, and take $\kappa = 0.4$.

Recently, an analysis of ATLAS data on W and Z production in pp collisions at the LHC claimed a significantly larger strange quark sea, with $\kappa \sim 1$ [37]. However, in a combined fit to data on charm production from neutrino DIS and from the LHC, Alekhin *et al.* [38] argued that the apparent strange quark enhancement is likely due to a corresponding suppression of the $\bar{d}$-quark PDF at small x. They point out that this reflects the limitations of attempts to separate individual quark flavor PDFs based solely on data from pp and ep scattering. Note that in all of these analyses the assumption is made that $s = \bar{s}$. Possible differences between the s and $\bar{s}$ PDFs can arise from both perturbative [39] and nonperturbative [40] effects and could affect, for example, the extraction of the weak mixing angle from neutrino data [41]. A detailed analysis of the strange

quark PDF using LHC and other data within the CJ framework will be performed in future work.

B. Heavy quarks

The existence of heavy quark PDFs in the nucleon introduces new mass scales and leads to the appearance of logarithmic terms of the form $\log Q^2/m_q^2$ in perturbative QCD calculations, where m_q is the mass of the heavy quark. As Q^2 grows these can become large and need to be resummed. The evolution equations for the PDFs sum these potentially large logarithms. In schemes where the heavy quarks are treated as massless in the hard scattering subprocesses, the heavy quark mass enters via the boundary conditions on the PDFs at the heavy quark threshold. Typically, this takes the form of imposing that the heavy quark PDF vanishes for Q^2 below m_q^2, with massless evolution being used as Q^2 increases. Although valid asymptotically, this result does not treat the threshold region correctly, since the threshold occurs in the variable W^2, not Q^2.

In this analysis, we are interested in determining the PDFs over ranges of Q^2 and x that include the threshold regions for the c and b quarks. To correctly treat these regions we implement the S-ACOT scheme as presented in Ref. [22]. This is a simplified version that is equivalent to the variable flavor ACOT scheme [42]. The S-ACOT scheme has been implemented for the neutral current DIS processes in the present analysis, and we take the masses of the charm and bottom quarks to be $m_c = 1.3$ GeV and $m_b = 4.5$ GeV, respectively.

C. $1/Q^2$ corrections

The cuts on Q^2 and W^2 imposed on the data sets used in this analysis (see Sec. III below) significantly increase the number of data points available to constrain PDFs. While this allows access to a greater range of kinematics and leads to reduced PDF uncertainties, especially at higher values of x, it also requires careful treatment of subleading, $\mathcal{O}(1/Q^2)$ power corrections to the leading-twist calculations. The most basic correction arises from imposing exact kinematics on twist-two matrix elements at finite values of Q^2, which gives rise to effects that scale with $x^2 M^2/Q^2$. These target mass corrections (TMCs) were first evaluated within the operator product expansion (OPE) [43] for DIS processes and allow structure functions at finite Q^2 to be expressed in terms of their $M^2/Q^2 \to 0$ (or "massless") values. For the F_2 structure function, for instance, one has [43–45]

$$F_2(x, Q^2) = \frac{(1+\rho)^2}{4\rho^3} F_2^{(0)}(\xi, Q^2) + \frac{3x(\rho^2 - 1)}{2\rho^4} \int_\xi^1 du$$
$$\times \left[1 + \frac{\rho^2 - 1}{2x\rho}(u - \xi) \right] \frac{F_2^{(0)}(u, Q^2)}{u^2}, \tag{5}$$

where $F_2^{(0)}$ is the structure function in the $M^2/Q^2 \to 0$ limit. Here the massless limit functions are evaluated in terms of the modified scaling variable ξ [46,47],

$$\xi = \frac{2x}{1+\rho}, \qquad \rho^2 = 1 + \frac{4x^2 M^2}{Q^2}, \qquad (6)$$

which approaches x as $M^2/Q^2 \to 0$.

Later work within the collinear factorization framework provided an alternative formulation of TMCs [48], which had the advantage that it could also be applied to processes other than inclusive DIS [49,50]. To $\mathcal{O}(1/Q^2)$, the two approaches can in fact be shown to be equivalent. A number of other prescriptions have also been proposed in the literature [44,51–54], using different approximations to the OPE and collinear factorization methods. In the context of a global PDF fit, it was found in Ref. [12] that differences arising from the various prescriptions can be effectively compensated by the presence of phenomenological higher-twist terms. In the present analysis, we use the standard OPE expression for the TMCs in Eq. (5).

For other subleading $1/Q^2$ corrections, which include higher twists but also other residual power corrections, we follow our earlier work [12–14] and parametrize the correction in terms of a phenomenological x-dependent function,

$$F_2(x, Q^2) = F_2^{\mathrm{LT}}(x, Q^2)\left(1 + \frac{C_{\mathrm{HT}}(x)}{Q^2}\right), \qquad (7)$$

where F_2^{LT} denotes the leading-twist structure function, including TMCs. The higher-twist coefficient function is parametrized by a polynomial function as

$$C_{\mathrm{HT}}(x) = h_0 x^{h_1}(1 + h_2 x), \qquad (8)$$

with h_0, h_1 and h_2 as free parameters. For simplicity, we assume the high-twist correction to be isospin independent (see, however, Refs. [55–58]); the possible isospin dependence of F_2 and other structure functions will be studied in a future dedicated analysis.

D. Nuclear corrections

As in the previous CJ PDF analyses [12–14], the use of deuterium DIS and Drell-Yan data necessitates taking into account the differences between PDFs in the deuteron and those in the free proton and neutron. The CJ15 analysis follows a similar approach, with several improvements over the earlier implementations, as we discuss in this section. While the earlier analyses applied nuclear corrections only to deep-inelastic deuteron structure functions, here we formulate the corrections at the parton level and generalize the treatment to any process involving quark, antiquark or gluon PDFs in the deuteron.

Generally, the nuclear corrections in high-energy reactions account for Fermi motion, binding, and nucleon off-shell effects, which are implemented in the form of convolutions with nuclear smearing functions. The nuclear effects become increasingly important at intermediate and large values of x, and will be the focus of this section. In addition, rescattering effects mediated by Pomeron and pion exchange mechanisms give rise to shadowing at small values of x ($x \lesssim 0.1$) [59,60] and a small amount of antishadowing at $x \sim 0.1$ [60,61]; in this analysis, we implement these using the results from Ref. [60]. In practice, however, the shadowing and antishadowing corrections are very small, and have negligible effect on the phenomenology considered in this paper.

1. Nuclear smearing

From the standard nuclear impulse approximation for the scattering of a projectile (lepton or hadron) from a deuteron d, the momentum distribution of a parton inside the deuteron is given by a convolution of the corresponding PDF in the bound nucleon and a momentum distribution $f_{N/d}$ of nucleons in the deuteron (or "smearing function"). Taking for illustration the PDF for a quark of flavor q (the generalization to antiquarks and gluons is straightforward), its parton momentum distribution in the deuteron can be computed as [62,63]

$$q^d(x, Q^2) = \int \frac{dz}{z} dp^2 f_{N/d}(z, p^2) \tilde{q}^N(x/z, p^2, Q^2), \qquad (9)$$

where $z = (M_d/M)(p \cdot q/p_d \cdot q)$ is the nucleon momentum fraction in the deuteron, with p and p_d the four-momenta of the nucleon and deuteron, respectively, and M_d is the deuteron mass. The nucleon virtuality p^2 defines the degree to which the bound nucleon is off its mass shell, $p^2 \neq M^2$, and the function $\tilde{q}^N$ represents the quark PDF in the off-shell nucleon. For the isoscalar deuteron, a sum over the nucleons $N = p$, n is implied. For inclusive DIS, the higher-twist contribution to the F_2^d structure function is computed analogously to Eq. (9), by convoluting the product of the off-shell nucleon parton distribution and the higher-twist function C_{HT} in Eq. (8) with the nucleon smearing function. For DY processes, the higher-twist component is very small and can be neglected [64].

While the off-shell nucleon PDF $\tilde{q}^N$ is not by itself an observable, its dependence on the virtuality p^2 can be studied within a given theoretical framework. Since the bound state effects in the deuteron are the smallest of all the atomic nuclei, one may expand the off-shell nucleon distribution to lowest order about its on-shell limit [63,65],

$$\tilde{q}^N(x, p^2, Q^2) = q^N(x, Q^2)\left(1 + \frac{p^2 - M^2}{M^2}\delta f^N(x, Q^2)\right), \qquad (10)$$

where the coefficient of the off-shell term is given by

$$\delta f^N(x, Q^2) = \frac{\partial \ln \tilde{q}^N(x, p^2, Q^2)}{\partial \ln p^2}\bigg|_{p^2=M^2}. \quad (11)$$

The on-shell term in Eq. (10) leads to the standard on-shell convolution representation for the nuclear PDF, while the off-shell term can be evaluated as an additive correction. Defining the total quark PDF in the deuteron as the sum of the on-shell and off-shell contributions, $q^d = q^{d(\text{on})} + q^{d(\text{off})}$, the two components can be written as

$$q^{d(\text{on})}(x, Q^2) = \int \frac{dz}{z} f^{(\text{on})}(z) q^N(x/z, Q^2), \quad (12\text{a})$$

$$q^{d(\text{off})}(x, Q^2) = \int \frac{dz}{z} f^{(\text{off})}(z) \delta f^N(x/z, Q^2) q^N(x/z, Q^2). \quad (12\text{b})$$

The on-shell and off-shell smearing functions $f^{(\text{on})}$ and $f^{(\text{off})}$ are taken to be the same for the proton and neutron (isospin symmetry breaking effects are not expected to be significant) and are given by [64]

$$f^{(\text{on})}(z) = \int dp^2 f_{N/d}(z, p^2), \quad (13\text{a})$$

$$f^{(\text{off})}(z) = \int dp^2 \frac{p^2 - M^2}{M^2} f_{N/d}(z, p^2). \quad (13\text{b})$$

A systematic method for computing the smearing functions is within the weak binding approximation, in terms of the deuteron wave function [66,67]. For large $Q^2 \to \infty$ the on-shell smearing function $f^{(\text{on})}$ has a simple probabilistic interpretation in terms of the light-cone momentum fraction $z \to (M_d/M)(p^+/p_d^+)$ of the deuteron carried by the struck nucleon, where $p^+ = p_0 + p_z$ is the "plus" component of the four-vector p. At finite Q^2, however, the smearing functions depend also on the parameter ρ^2, which characterizes the deviation from the Bjorken limit, and the momentum fraction variable is $z = 1 + (\varepsilon + \rho p_z)/M)$, where $\varepsilon = p_0 - M$ is the separation energy. In fact, the ρ dependence of the smearing functions is different for the F_1 and F_2 DIS structure functions, and for Drell-Yan cross sections, so that the convolutions at finite Q^2 depend on the deuteron observable that is being computed.

For the deuteron wave functions, we consider several modern potentials based on high-precision fits to nucleon-nucleon scattering data. The models differ primarily in their treatment of the short-range NN interaction, while the long-range part of the wave functions is constrained by the chiral symmetry of QCD and parametrized through one-pion exchange. Specifically, the nonrelativistic AV18 [68] and CD-Bonn [69] NN potential models (which fit around 3,000 data points in terms of $\approx$40 parameters), and the more recent relativistic WJC-1 and WJC-2 [70] potentials (which describe almost 4,000 data points in terms of 27 and 15 parameters, respectively), provide wave functions with a representative spread of behaviors in the low- and high-momentum regions. Of these, the CD-Bonn wave function has the softest momentum distribution, while the WJC-1 wave function has the hardest, with the others lying between the two. The differences in the strength of the high-momentum tails of the wave functions are reflected in differences between the behaviors of the nuclear corrections at large values of x. Note that the effects of the nuclear smearing corrections are not suppressed at large Q^2 and must be considered at all scales wherever data at $x \gtrsim 0.3$ are used [12,71,72].

2. Nucleon off-shell corrections

While the effects of the nuclear smearing are relatively well understood, at least in the sense that they can be directly related to the properties of the deuteron wave function, the nucleon off-shell correction in Eqs. (10) and (11) is much more uncertain and model dependent. In the literature, a number of model studies have been performed to estimate the modification of PDFs in bound nucleons relative to the free nucleon PDFs [62,63,65,66,73–77], some of which have been motivated by the original observation of the nuclear EMC effect [78] (namely, the deviation of the nuclear to deuterium structure function ratio from unity).

Some early studies of off-shell corrections to PDFs were based on spectator quark models [62,63,65,66,74], in which the scattering takes place from a quark that is accompanied by a "diquark" system (proton with a quark removed) that is a spectator to the deep-inelastic collision. The scattering amplitude was represented through a quark spectral function characterized by an ultraviolet momentum cutoff scale Λ and an invariant mass of the spectator system, both of which were fixed by comparing with the on-shell structure function data.

The effects of nucleon off-shell corrections on global PDF analysis were explored in the CTEQ6X analysis [12] using a simple analytic parametrization of the corrections computed in the relativistic quark spectator model of Ref. [74]. In the subsequent CJ11 analysis [13], a more elaborate off-shell model was considered [66], in which the corrections were related to the change in the nucleon's confinement radius in the nuclear medium, as well as the average virtuality of the bound nucleons. The change in the confinement radius (or nucleon "swelling") ranged between 1.5% and 1.8%, and the virtuality of the bound nucleons $\langle p^2 - M^2 \rangle / M^2 \equiv \int dz f^{(\text{off})}(z)$ was independently varied between -3.6% to -6.5% for the four deuteron wave functions discussed above.

Most recently, the CJ12 global analysis [14] further took into account the correlations between the nucleon swelling

and the deuteron wave function, defining a set of nuclear corrections that ranged from mild (for the hardest, WJC-1 wave function [70] coupled to a small, 0.3% nucleon swelling) to strong (for the softest, CD-Bonn wave function [69] with a large, 2.1% swelling parameter). The entire range of nuclear corrections was consistent with the existing experimental data, with each of the CJ12min, CJ12mid and CJ12max PDF sets giving essentially the same χ^2 values for the global fit, $\chi^2/\text{datum} \approx 1.03$.

In the present CJ15 analysis, in order to decrease the model dependence of the off-shell correction and increase the flexibility of the fit, we follow the proposal of Kulagin and Petti [66] and employ a phenomenological parametrization with parameters fitted to data. From the constraint that the off-shell correction does not modify the number of valence quarks in the nucleon,

$$\int_0^1 dx \delta f^N(x)[q(x) - \bar{q}(x)] = 0, \qquad (14)$$

one can infer that the function δf^N must have one or more zeros in the physical range between $x = 0$ and 1. We can, therefore, take the off-shell function δf^N to be parametrized by the form

$$\delta f^N = C(x - x_0)(x - x_1)(1 + x_0 - x), \qquad (15)$$

with the zeros x_0 and x_1 and normalization C free parameters. In practice, we fit the zero crossing parameter x_0 and the normalization C, which then allows the second zero crossing x_1 to be determined from Eq. (14) analytically. In Ref. [66], these parameters were constrained by fitting to ratios of nuclear to deuteron structure function data, for a range of nuclei up to ^{207}Pb. This resulted in a combined nuclear correction that produced a ratio of deuteron to nucleon structure functions F_2^d/F_2^N with a shape similar to that for heavy nuclei [78,79], including an $\approx 1\%$ antishadowing enhancement in F_2^d/F_2^N at $x \approx 0.1$–0.2. In contrast, in the present analysis, we fit the off-shell parameters by considering only deuterium cross section data and their interplay with proton data for a range of processes sensitive to the d-quark PDF.

To test the sensitivity of the fit to the off-shell parametrization, we also consider as an alternative the model of Ehlers *et al.* [64], who generalized the quark spectator model employed in the CJ12 analysis [14] to allow for different off-shell behaviors of the valence quark, sea quark and gluon distributions. In previous studies the off-shell corrections were implemented only for the deuteron F_2^d structure function and in the valence quark approximation. The generalized model [64], on the other hand, which we refer to as the "off-shell covariant spectator" (OCS) model, can be applied to observables that are sensitive to both the valence and sea sectors, such as the deuteron F_L^d structure function or proton–deuteron Drell-Yan cross sections.

More specifically, in the OCS model, three masses for the respective spectator states ("qq" for valence quarks, "$qq\bar{q}q$" for sea quarks, and "qqq" for gluons) were fitted to the isoscalar valence, sea quark and gluon PDFs in the free nucleon. The only free parameter in the model is the rescaling parameter $\lambda = \partial \log \Lambda^2 / \partial \log p^2$, evaluated at $p^2 = M^2$. The variable λ can then be included as a parameter in the fit, with errors propagated along with those of the other leading-twist parameters.

Finally, we note that in a purely phenomenological approach adopted by Martin *et al.* [80], the entire deuterium nuclear correction is parametrized by a Q^2-independent function, without appealing to physical constraints. To mock up the effects of Fermi motion, the parametrization includes a logarithm raised to a high power, $\sim \ln^{20}(x)$, which produces the steep rise in the F_2^d/F_2^N ratio at high x. In the convolution formula in Eq. (9), this effect arises naturally from the smearing of the nucleon structure function by the nucleon momentum distribution function $f_{N/d}$.

III. DATA

The CJ15 PDFs are obtained by fitting to a global database of over 4500 data points from a variety of high-energy scattering processes, listed in Table I. These include deep-inelastic scattering data from BCDMS [81], SLAC [82], NMC [83,84], HERA [85], HERMES [86] and Jefferson Lab [20,21,87], Drell-Yan pp and pd cross sections from fixed target experiments at Fermilab [29], W [17–19,88,89] and Z [90,91] asymmetries, as well as jet [92,93] and $\gamma + \text{jet}$ [94] cross sections from the CDF and DØ Collaborations at the Tevatron. Cuts on the kinematic coverage of the DIS data have been made for $Q^2 > Q_0^2 = 1.69 \text{ GeV}^2$ and $W^2 > 3 \text{ GeV}^2$, as in the CJ12 analysis [14]. Compared with the CJ12 fit, however, several new data sets are included in the new analysis.

For DIS, we include the new results from the BONuS experiment [20,21] in Jefferson Lab's Hall B, which collected around 200 data points on the ratio of neutron to deuteron F_2 structure functions up to $x \approx 0.6$, using a spectator tagging technique to isolate DIS events from a nearly free neutron inside a deuterium nucleus [75]. Unlike all previous extractions of neutron structure from deuterium targets, which have been subject to large uncertainties in the nuclear corrections in the deuteron at high x [16,67], the BONuS data provide the first direct determination of F_2^n in the DIS region, essentially free of nuclear uncertainties.

New data sets from the run II of HERA [4,85] and from HERMES on the proton and deuteron structure functions [86] have become available recently, and are included in this analysis. During the fitting process it was noted that the HERMES data from the highest-Q^2 bin (bin "F" [86]) differed significantly from results from other experiments in the same kinematic region, and in the final analysis the

TABLE I.   Data sets used in the CJ15 global analysis, with the corresponding number of data points and χ^2 values for each set. The main CJ15 NLO fit (in boldface), which uses the AV18 deuteron wave function and off-shell parametrization in Eq. (15), is compared with an LO fit and NLO fits with the OCS off-shell model, no nuclear corrections, and no nuclear corrections or DØ W asymmtetry data.

Observable	Experiment	# points	χ^2				
			LO	NLO	NLO (OCS)	NLO (no nucl)	NLO (no nucl/D0)
DIS F_2	BCDMS (p) [81]	351	426	**438**	436	440	427
	BCDMS (d) [81]	254	292	**292**	289	301	301
	SLAC (p) [82]	564	480	**434**	435	441	440
	SLAC (d) [82]	582	415	**376**	380	507	466
	NMC (p) [83]	275	416	**405**	404	405	403
	NMC (d/p) [84]	189	181	**172**	173	174	173
	HERMES (p) [86]	37	57	**42**	43	44	44
	HERMES (d) [86]	37	52	**37**	38	36	37
	Jefferson Lab (p) [87]	136	172	**166**	167	177	166
	Jefferson Lab (d) [87]	136	131	**123**	124	126	130
DIS F_2 tagged	Jefferson Lab (n/d) [21]	191	216	**214**	213	219	219
DIS σ	HERA (NC $e^- p$) [85]	159	315	**241**	240	247	244
	HERA (NC $e^+ p$ 1) [85]	402	952	**580**	579	588	585
	HERA (NC $e^+ p$ 2) [85]	75	177	**94**	94	94	93
	HERA (NC $e^+ p$ 3) [85]	259	311	**249**	249	248	248
	HERA (NC $e^+ p$ 4) [85]	209	352	**228**	228	228	228
	HERA (CC $e^- p$) [85]	42	42	**48**	48	45	49
	HERA (CC $e^+ p$) [85]	39	53	**50**	50	51	51
Drell-Yan	E866 (pp) [29]	121	148	**139**	139	145	143
	E866 (pd) [29]	129	202	**145**	143	158	157
W/charge asymmetry	CDF (e) [88]	11	11	**12**	12	13	14
	DØ (μ) [17]	10	18	**20**	19	29	28
	DØ (e) [18]	13	49	**29**	29	14	14
	CDF (W) [89]	13	16	**16**	16	14	14
	DØ (W) [19]	14	35	**14**	15	82	—
Z rapidity	CDF (Z) [90]	28	108	**27**	27	26	26
	DØ (Z) [91]	28	26	**16**	16	16	16
jet	CDF (run 2) [92]	72	29	**15**	15	23	25
	DØ (run 2) [93]	110	87	**21**	21	14	14
γ + jet	DØ 1 [94]	16	16	**7**	7	7	7
	DØ 2 [94]	16	34	**16**	16	17	17
	DØ 3 [94]	12	35	**25**	25	24	25
	DØ 4 [94]	12	79	**13**	13	13	13
total		4542	5935	**4700**	4702	4964	4817
total + norm			6058	**4708**	4710	4972	4826
χ^2/datum			1.33	**1.04**	1.04	1.09	1.07

data in the Q^2 bin F were not included. The other DIS data sets are unchanged from those used in the CJ12 analysis [14].

For the Drell-Yan data from the E866 experiment [29] at Fermilab, following the suggestion in Ref. [95] we employ a cut on the dimuon cross sections for dimuon masses $M_{\mu^+\mu^-} > 6$ GeV. This reduces the number of data points from 375 to 250 compared to the usual cut of $M_{\mu^+\mu^-} \gtrsim 4$ GeV, but leads to a significant reduction in the χ^2/datum for those data. In previous fits, dimuon data from the E605 Drell-Yan experiment at Fermilab [96] were also used. However, those data were taken on a copper target and are therefore potentially subject to nuclear corrections. Since the nuclear corrections used in the

CJ15 fit pertain only to deuterium targets, we have chosen not to use the E605 data in this analysis.

Several new data sets from W-boson production in pp collisions at the Tevatron have also recently become available and are included in the CJ15 fit. New data from the DØ Collaboration on muon [17] and electron [18] charge asymmetries supersede previous lepton asymmetry measurements, and remove the tension with the extracted W-boson asymmetries that was evident in our previous CJ12 analysis [14]. The new W-boson asymmetry data from DØ [19] have about 10 times larger integrated luminosity, and extend over a larger W-boson rapidity range, up to ≈ 3, than the earlier CDF measurement [89]. While the lepton asymmetry data are more sensitive to

PDFs at small values of x, the W-boson asymmetry data at large rapidities generally provide stronger constraints on PDFs at large x values.

IV. RESULTS

In this section, we present the results of our global QCD analysis. The quality of the fit to the data is illustrated in Fig. 1, where the inclusive proton F_2 structure functions from BCDMS [81], SLAC [82], NMC [83] and HERMES [86] are compared with the CJ15 NLO fit as a function of Q^2 at approximately constant values of x. In Fig. 2, the Jefferson Lab F_2^p data from the E00-116 experiment in Hall C [87] are compared with the CJ15 results at fixed

scattering angles, with x increasing with Q^2. The more recent data from the BONuS experiment at Jefferson Lab [21] on the ratio of neutron to deuteron structure functions, F_2^n/F_2^d, are shown in Fig. 3. Overall the agreement between the theory and data, over several decades of Q^2 and x, is excellent.

The uncertainties on the observables in Figs. 1–3 (and on the PDFs throughout this paper, unless otherwise noted) are computed using Hessian error propagation, as outlined in Ref. [14], with $\Delta\chi^2 = 2.71$, which corresponds to a 90% confidence level (C.L.) in the ideal Gaussian statistics. The corresponding χ^2 values for each of the data sets in Figs. 1–3, and all other data used in the fits, are listed in Table I. As well as the main NLO fit, we also include the χ^2
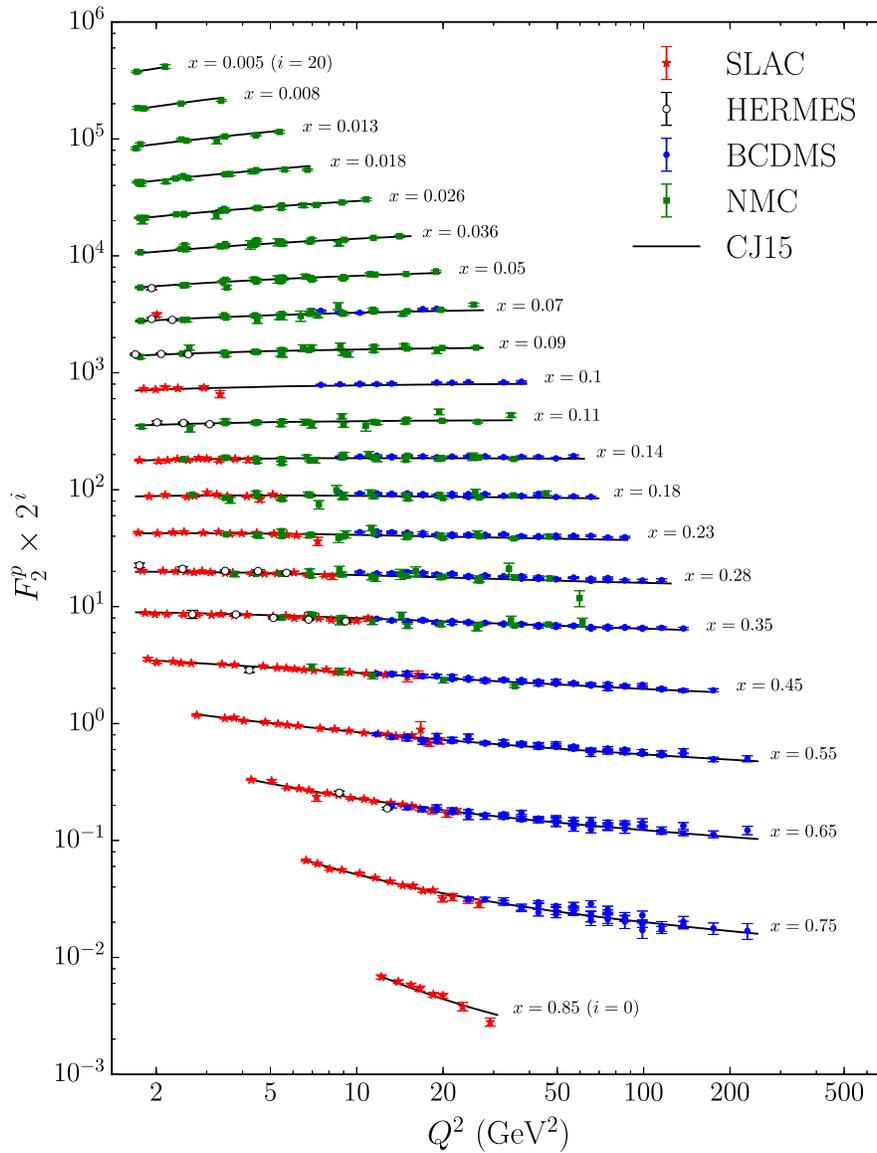
FIG. 1.   Comparison of proton F_2^p structure function data from BCDMS [81], SLAC [82], NMC [83] and HERMES [86] with the CJ15 fit, as a function of Q^2 for approximately constant x. The data have been scaled by a factor 2^i, from $i = 0$ for $x = 0.85$ to $i = 20$ for $x = 0.005$, and the PDF uncertainties correspond to a 90% C.L.
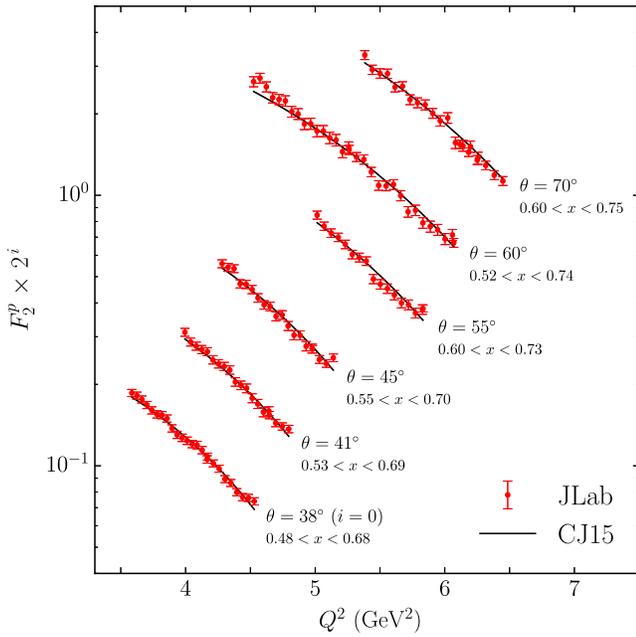
FIG. 2. Comparison of the proton F_2^p structure function data from the E00-116 experiment in Jefferson Lab (JLab) Hall C [87] with the CJ15 fit, as a function of Q^2 for fixed scattering angle θ, with the corresponding x ranges indicated. The data have been scaled by a factor 2^i, from $i = 0$ for $\theta = 38°$ to $i = 5$ for $\theta = 70°$, and the PDF uncertainties correspond to a 90% C.L.
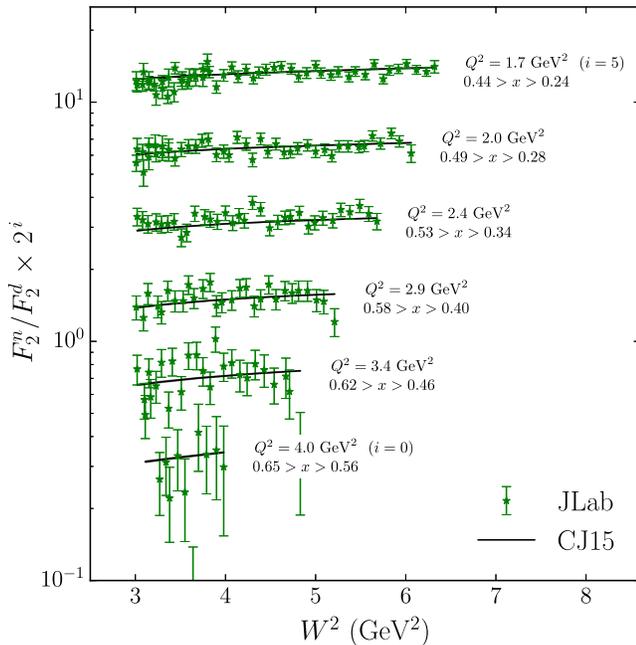

FIG. 3. Comparison of the F_2^n/F_2^d structure function ratio from the BONuS experiment in Jefferson Lab (JLab) Hall B [21] with the CJ15 fit, as a function of the invariant mass W^2 for fixed Q^2, with the corresponding x ranges indicated (note x decreases with increasing W^2). The data have been scaled by a factor 2^i, from $i = 0$ for $Q^2 = 4.0$ GeV^2 to $i = 5$ for $Q^2 = 1.7$ GeV^2, and the PDF uncertainties correspond to a 90% C.L.

values for several alternate fits, with different combinations of theory and data (see below), and an LO fit. For the central NLO fit, the total χ^2 is $\approx$4700 for 4542 points, or $\chi^2/\text{datum} = 1.04$, which is similar to our previous CJ12 analysis [14], even though that fit was to some 500 fewer points. While the various NLO fits give qualitatively similar χ^2 values, the χ^2/datum for the LO fit ($\sim$1.3) is markedly worse.

A. CJ15 PDFs

The CJ15 PDFs themselves are displayed in Fig. 4 at a scale of $Q^2 = 10$ GeV^2 for the u, d, $\bar{d} + \bar{u}$, $\bar{d} - \bar{u}$ and s distributions, and the gluon distribution scaled by a factor $1/10$. The central CJ15 PDFs are determined using the AV18 deuteron wave function and the nucleon off-shell parametrization in Eq. (15). The parameter values and their 1σ errors for the leading-twist distributions at the input scale Q_0^2 are given in Table II, with the parameters that are listed without errors fixed by sum rules or other constraints. (To avoid rounding errors when using these values in numerical calculations, we give each of the parameter values and their uncertainties to five significant figures.)

The strange quark PDF is assumed in this analysis to be proportional to the light antiquark sea in the ratio $\kappa = 0.4$ [see Eq. (4)]. To test the sensitivity of our fit to the specific value of κ, we repeated the analysis varying the strange to nonstrange quark ratio between 0.3 and 0.5. Within this range the total χ^2 spans between 4704 ($\kappa = 0.3$) and 4711 ($\kappa = 0.5$), indicating a very weak dependence on κ. This is not surprising given that our analysis does not include any data sets that are particularly sensitive to the strange-quark PDF.
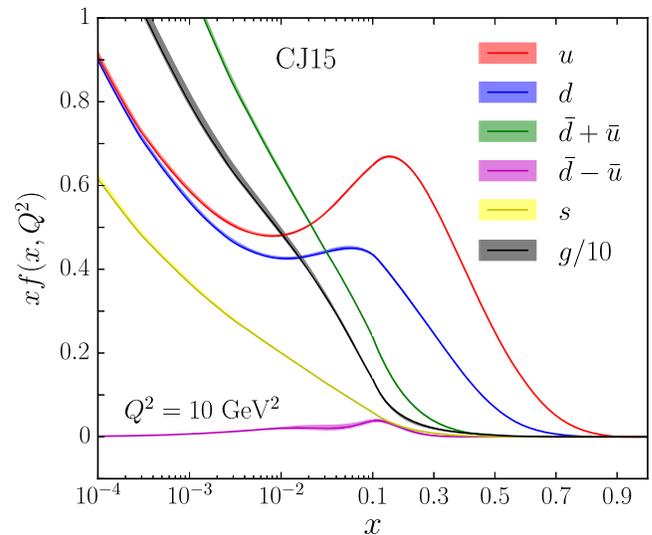

FIG. 4. Comparison of CJ15 PDFs $xf(x, Q^2)$ for different flavors ($f = u$, d, $\bar{d} + \bar{u}$, $\bar{d} - \bar{u}$, s and $g/10$) at a scale $Q^2 = 10$ GeV^2, with 90% C.L. uncertainty bands. Note the combined logarithimic/linear scale along the x-axis.

TABLE II. Leading-twist parameter values and the 1σ uncertainties for the u_v, d_v, $\bar{d} + \bar{u}$, $\bar{d}/\bar{u}$ and g PDFs [Eqs. (1), (3)] from the CJ15 NLO analysis at the input scale Q_0^2. Parameters without errors have been fixed. For the d_v PDF, the large-x parameters [Eq. (2)] are given by $b = (3.6005 \pm 0.66324) \times 10^{-3}$ with $c = 2$. For the strange to nonstrange sea quark PDF ratio [Eq. (4)], we take $\kappa = 0.4$. (The parameter values are given to five significant figures to avoid rounding errors.).

Parameter	u_v	d_v	$\bar{d} + \bar{u}$	$\bar{d}/\bar{u}$	g
a_0	2.4067	24.684	0.14658 ± 0.0050348	35712	45.542
a_1	0.61537 ± 0.019856	1.1595 ± 0.033533	-0.20775 ± 0.0037551	4.0249 ± 0.07407	0.60307 ± 0.031164
a_2	3.5433 ± 0.012414	6.5514 ± 0.15936	8.3286 ± 0.19114	20.154 ± 0.87862	6.4812 ± 0.96748
a_3	0	-3.5030 ± 0.086332	0	17	-3.3064 ± 0.13418
a_4	3.4609 ± 0.42903	4.6787 ± 0.14209	14.606 ± 1.2151	51.156 ± 10.239	3.1721 ± 0.31376

PDFs for other flavors, such as charm and bottom, are not shown in Fig. 4. The heavy quark distributions are generated perturbatively through Q^2 evolution. While there has been speculation about nonperturbative or intrinsic contributions to heavy flavor PDFs, there is currently no evidence from global analysis of high-energy scattering data to suggest that these are large [97]. Until more conclusive evidence becomes available, it is reasonable to set these equal to zero. This is in contrast with the light quark sea, for which a nonperturbative component at the input scale is essential to account for the nonzero flavor asymmetry $\bar{d} - \bar{u}$.

To study the effect of using the S-ACOT prescription for the c and b quarks, the results for the CJ15 PDFs were compared to those obtained using the zero-mass variable flavor number (ZMVFS) scheme. As expected, the changes to the u and d PDFs were modest, typically less than 2%. On the other hand, an enhancement of up to 40% was observed for large values of $x \sim 0.4$ for both the gluon and charm PDF (which are coupled by Q^2 evolution). For the $\bar{u}$ and $\bar{d}$ PDFs there was an approximately 5% increase near $x \approx 0.1$, followed by a decrease at larger values of x. However, these effects largely canceled in the $\bar{d}/\bar{u}$ ratio.

The default value for the five-flavor strong QCD scale parameter used in our analysis is $\Lambda_{\rm QCD}^{(5)} = 0.2268$ GeV, corresponding to $\alpha_s(M_Z) = 0.1180$. This may be compared to the world average values quoted by the Particle Data Group, $\Lambda_{\rm QCD}^{(5)} = (0.2303 \pm 0.0006)$ GeV and $\alpha_s(M_Z) = 0.1185 \pm 0.0006$ [98]. Repeating our standard analysis with $\Lambda_{\rm QCD}^{(5)}$ treated as a free parameter, on the other hand, yields $\Lambda_{\rm QCD}^{(5)} = (0.230 \pm 0.002)$ GeV and $\alpha_s(M_Z) = 0.1183 \pm 0.0002$, which are compatible with the PDG results.

The CJ15 distributions are compared with PDFs from several recent representative NLO global parametrizations in Fig. 5, in the form of ratios to the central CJ15 distributions. Since different PDF analyses typically utilize different criteria for estimating PDF errors, we display the CJ15 errors for the standard $\Delta\chi^2 = 1$, or 68% C.L. for Gaussian statistics, as well as with $\Delta\chi^2 = 2.71$, or

90% C.L. Generally the MMHT14 [6] PDF set, which uses a dynamical tolerance criteria, and the NNPDF3.0 [8] set have larger PDF uncertainties than CJ15. The PDFs uncertainties from HERAPDF1.5 [9] are closer to the CJ15 68% errors, which may be expected given that the HERAPDF1.5 analysis only fits HERA data and uses the $\Delta\chi^2 = 1$ criterion for generating errors.

For the u-quark PDF, the results from different parametrizations are generally within 5% for $x \lesssim 0.5$, with the exception of the HERAPDF1.5 set, which is up to $\approx 10\%$ larger at $x \approx 10^{-2}$. At $x \gtrsim 0.6$, where data are more limited, there is larger deviation among the PDF sets, although the uncertainties are correspondingly larger. A somewhat greater spread between the different parametrizations is found for the d-quark PDF, with the NNPDF3.0 and HERAPDF1.5 results up to 10%–20% lower than CJ15 at $x \sim 0.3$–0.6, while the MMHT14 distribution generally follows CJ15.

As known from previous analyses, the relative uncertainties on the d-quark PDFs are significantly larger than those on the u-quark PDF, especially at large x. For the $\bar{u}$ and $\bar{d}$ distributions the results from the CJ15 fit are similar to those from the MMHT14 and NNPDF3.0 analyses, while the HERAPDF1.5 fit gives rather different results beyond $x \approx 0.1$–0.2. Note that the $\bar{d}/\bar{u}$ ratio is most strongly constrained by the E866 Drell-Yan pp and pd scattering data.

For the strange quark PDF, the uncertainties in CJ15 are somewhat smaller than for MMHT14 and NNPDF3.0. This is mostly due to the fact that the CJ15 s-quark PDF is assumed to scale with the light antiquark sea in the ratio $\kappa = 0.4$, while other analyses attempt to constrain s-quark PDF from neutrino data, which typically have much larger uncertainties. The errors on the gluon distribution in the MMHT14 and NNPDF3.0 fits are comparable to the 90% C.L. CJ15 errors, while the HERAPDF1.5 uncertainties are similar to the 68% C.L. CJ15 results. Uncertainties in other modern PDF analyses, such as CT14 [7], JR14 [10] or ABM11 [99], are generally between the representative sets illustrated in Fig. 5.
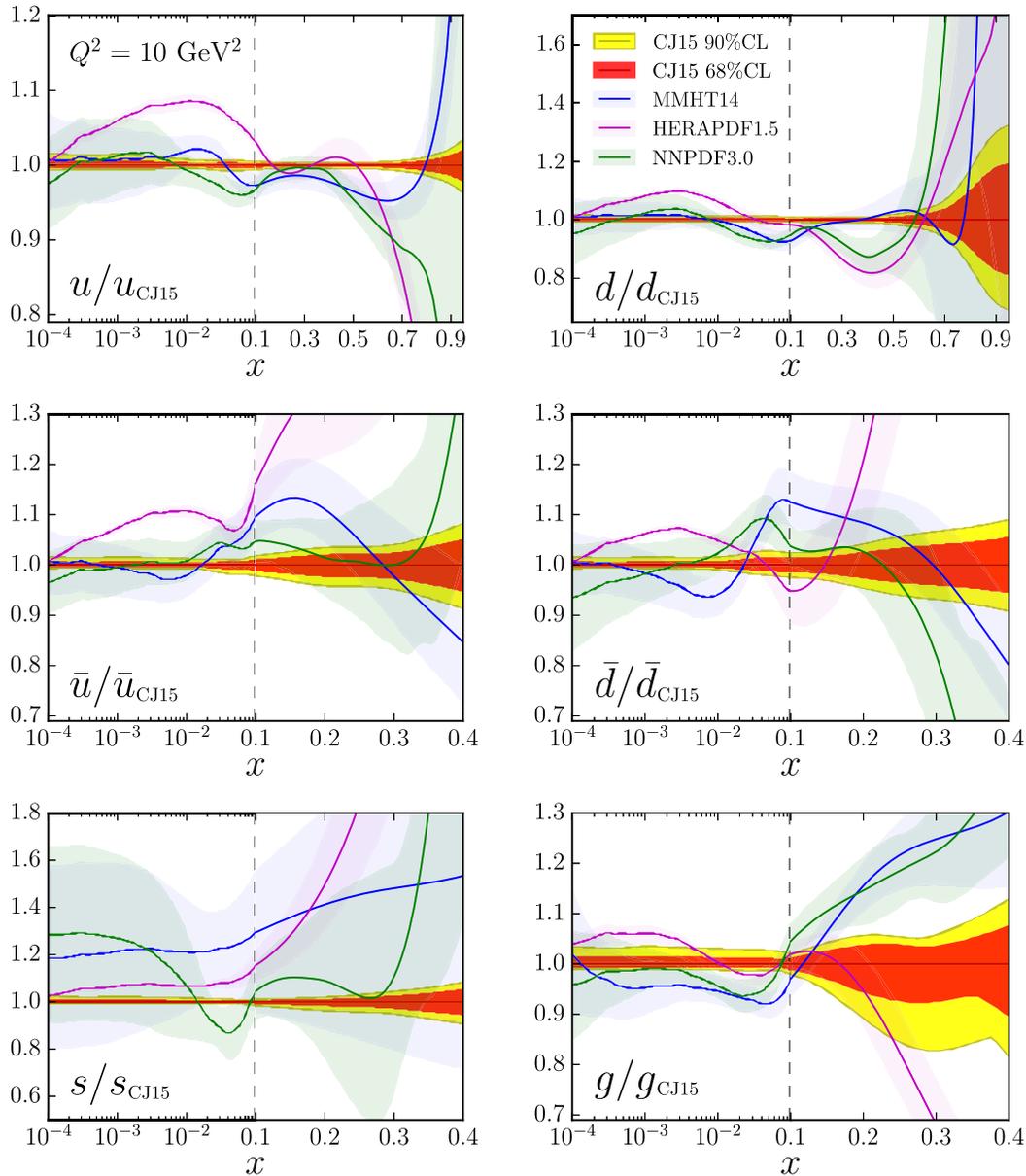
FIG. 5.   Ratio of PDFs to the CJ15 central values for various PDF sets: CJ15 with 90% C.L. (yellow) and 68% C.L. (red) uncertainty bands, MMHT14 [6] (blue), HERAPDF1.5 [9] (magenta), and NNPDF3.0 [8] (green). Note the different scales on the vertical axes used for different flavors.

B. Impact of new data sets and interplay of proton and nuclear data

The impact of the combined HERA run I and II inclusive proton DIS cross sections [85] has been discussed recently in Ref. [100], with particular focus on the small-x region. Compared to only using data from run I, we also find rather stable PDF central values. In the large-x region, the improvement in the PDF uncertainty is ~10% for the u distribution at $x \approx 0.05$–0.7, ~5% for the d distribution at $x \approx 0.05$–0.4 (and slightly less for the d/u ratio because of anticorrelations between these), and ~5% for the gluon PDF at $x \approx 0.05$–0.5. The influence of the HERMES data

on the proton and deuteron F_2 structure functions is less pronounced. These data induce a minor reduction, of less than 5%, in the uncertainty on the u and d PDFs at $x \lesssim 0.2$, which shrinks to less than 2% in the d/u ratio. This is due in part to the limited number of data points surviving our cuts, and the relatively large systematic errors compared with the other DIS data sets.

The most notable impact of the new data sets on the CJ15 fit is from the high-precision DØ data on the reconstructed W charge asymmetry [19]. These data allow us to simultaneously reduce the uncertainty on the d-quark PDF at $x \gtrsim 0.4$ by ~50% and fit the off-shell correction δf^N in Eq. (10).

This is possible only in the context of a global fit, by considering simultaneously the W asymmetry and deuteron DIS structure functions. If the d-quark PDF in the free nucleon can be determined with sufficient precision, the deuteron DIS data can then be used to constrain the nuclear corrections, and in particular, for a given deuteron wave function, the off-shell correction δf^N. In principle, the Jefferson Lab BONuS data [20,21] on quasifree neutrons can play an analogous role. Unfortunately, the statistics and kinematic reach at large x of the current data make this difficult, although future data from several planned experiments [101–103] at the energy-upgraded Jefferson Lab are expected to cover the required range in x with high precision.

This interplay between the proton and nuclear observables is already evident at the χ^2 level from Table I. When fitting data without including any nuclear corrections, significantly worse χ^2 values are obtained for the SLAC deuteron F_2 measurement and the DØ W asymmetry, in particular, increasing by 131 units over 582 points and 68 units over 14 points, respectively. Similar results are obtained when using the OCS model for the off-shell corrections instead of the parametrization in Eq. (10). Without nuclear corrections, a strong tension exists between the d-quark PDF constrained by one or the other of these observables. This is the first direct indication from a global PDF fit of the necessity of nuclear corrections, and opens the way for utilizing proton data to study the dynamics of partons in nuclei [23,104].

After including nuclear corrections, the DØ W asymmetry data can be fitted with $\chi^2/\text{datum} \approx 1$, and the SLAC deuteron F_2 data gives an even smaller χ^2 than that obtained when fitting with no corrections and no DØ data. The tension between these data sets is therefore completely removed by accounting for nuclear effects. Interestingly, the fit without nuclear corrections improves the χ^2 for the DØ muon asymmetry data [17], but gives a worse fit to the DØ electron asymmetry data [18]. Although less dramatically, nuclear corrections also improve the fit to the E886 pd Drell-Yan data.

Overall, it is encouraging that such a relatively simple parametrization for the nucleon off-shell corrections as used in this analysis is able to capture most of the effects in DIS and Drell-Yan observables, in which both valence and sea quarks play a role. With the upcoming data from the SeaQuest experiment at Fermilab [31] (and in the future from JPARC, as well as from dilepton, W and Z boson measurements in pd collisions at RHIC), separation of off-shell effects in the valence and sea quark sectors may become feasible.

C. Nuclear corrections at large x

As observed in Fig. 5, the uncertainty on the d-quark distribution at large x values ($x \gtrsim 0.3$) is generally much larger compared with that on the u-quark PDF. This reflects

the considerably greater quantity of high-precision proton F_2 structure function data, which, because of the larger charge on the u quark, is at least an order of magnitude more sensitive to the u-quark PDF than to the d. Traditionally, stronger constraints on the d-quark PDF have been sought from inclusive DIS from the neutron, in which the roles of the u and d quark are reversed relative to the proton. However, the absence of free neutron targets has meant that neutron structure information has had to be extracted from measurements on deuterium nuclei. Unfortunately, at high values of x ($x \gtrsim 0.5$) bound state effects in the deuteron become important, and uncertainties in their computation become progressively large with increasing x.

The effects of nuclear corrections on the PDFs are illustrated in Fig. 6, where fits using several different deuteron wave function models are compared. The distributions are displayed relative to the central CJ15 PDFs which use the AV18 deuteron wave function. All the fits employ the phenomenological nucleon off-shell parametrization in Eq. (15), with the parameters given in Table III for the AV18 deuteron wave function. The results using the CD-Bonn wave function are very similar to those for the AV18 wave function, while the WJC-1 and WJC-2 models lead to slightly larger differences in some of the PDFs shown in Fig. 6. On the other hand, the χ^2 values for the AV18, CD-Bonn and WJC-2 models are almost indistinguishable, with the WJC-1 model giving a marginally larger total χ^2 (4714 instead of 4700). This suggests that, for the most part, the nucleon off-shell parametrization in Eq. (15) is sufficiently flexible to compensate for changes induced by these wave functions. For the WJC-1 model it is a little more difficult for the off-shell corrections to compensate for this wave function's harder momentum distribution (relative to the other models) within the constraints of Eq. (15), and this leads to a slightly worse overall fit. Observables separately sensitive to the nucleon off-shellness, such as deuteron target DIS with a large momentum detected spectator, would be needed to separate these two effects.

As expected, the variations due to the nuclear models have the largest effects in the d-quark distribution, which is less constrained by proton data and hence more sensitive to uncertainties in the extracted neutron structure function. The spread in the d-quark PDF at $x = 0.8$ is $\approx 20\%$ between the four wave functions. The variations for the AV18 and CD-Bonn wave functions are generally within the $\Delta\chi^2 = 1$ C.L., while for the WJC-2 model the u and $\bar{u}$ distributions show the biggest deviations, in the vicinity of $x \sim 0.1$–0.2. For the WJC-1 deuteron model, the d-quark PDF is suppressed at high x relative to that in the other models, which correlates with the harder smearing function $f_{N/d}$ at large values of the nucleon light-cone momentum y and hence a larger F_2^d/F_2^N ratio at high x. As already noted in the CJ11 analysis [13], there is an anti-correlation
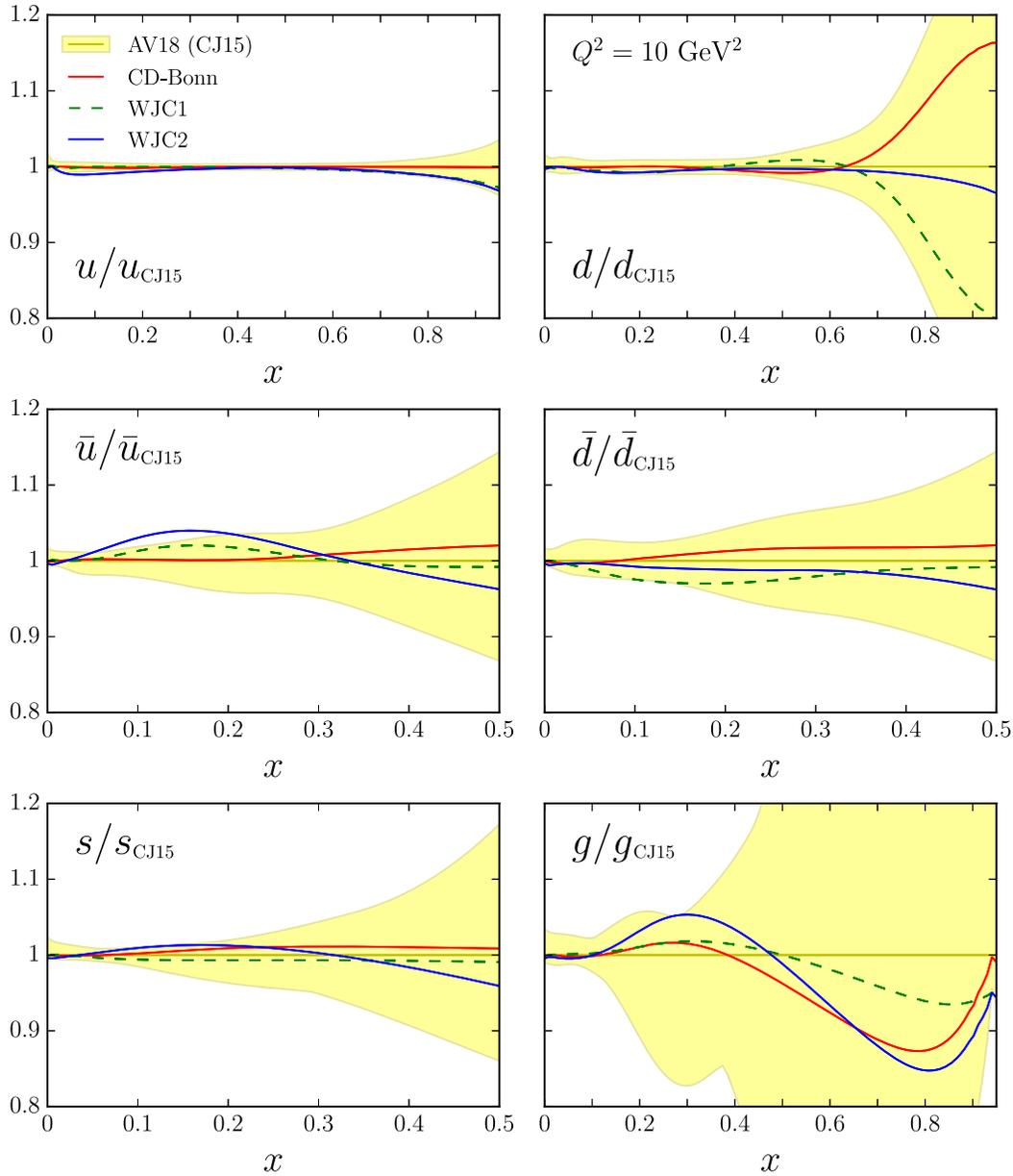
FIG. 6.   Ratio of PDFs fitted using various deuteron wave function models to the CJ15 PDFs (which use the AV18 deuteron wave function): CD-Bonn (solid red curves), WJC-1 (dashed green curves), WJC-2 (solid blue curves). The CJ15 PDFs (yellow band) correspond to a 90% C.L., and the off-shell parametrization (15) is used for all cases.

between the behavior of the *d*-quark distribution at large *x* and the gluon PDF. In fact, using the WJC-1 wave function leads to a slight decrease in all the quark PDFs at high *x* (within the range constrained by the data), while the gluon PDF has the opposite trend. The spread in the gluon PDF is $\lesssim 10\%$ for $x < 0.7$, although beyond $x \approx 0.3$ the gluon distribution has a very large uncertainty.

Note that while in Fig. 6 the same functional form from Eq. (15) is used for all fits, the off-shell parameters are refitted for each different deuteron wave function model, thereby absorbing most of the effect of the varying strength of the nucleon's momentum distribution tail. The fitted

off-shell functions δf^N are shown in Fig. 7 for the four wave function models considered. The off-shell corrections for the AV18, CD-Bonn and WJC-2 models have similar shapes: quite small at low *x*, but more negative at larger *x*, with magnitude peaking at $x \sim 0.8$. The function δf^N for these models has zero crossings at $x = x_1 \approx 0.05$ and $x = x_0 \approx 0.35$. For the WJC-1 model, on the other hand, the off-shell function is somewhat orthogonal to the others, becoming negative at lower *x* values and positive at higher $x \gtrsim 0.4$.

To test the sensitivity of the fit to the choice of off-shell model, we also consider the more microscopic OCS model

TABLE III. Parameter values and 1σ uncertainties for the nucleon off-shell [Eq. (15)] and higher twist [Eq. (8)] corrections to F_2 from the CJ15 NLO analysis at the input scale Q_0^2. The off-shell parameters are fitted using the AV18 deuteron wave function. Parameters without errors have been fixed. (The parameter values are given to five significant figures to avoid rounding errors.) The covariance matrix is provided for all the fitted off-shell and higher twist parameters.

Parameter	Value	Covariance matrix		
C	-3.6735 ± 1.5278	1.000	-0.173	
x_0	$(5.7717 \pm 1.4842) \times 10^{-2}$	-0.173	1.000	
x_1	0.36419			
h_0	-3.2874 ± 0.26061	1.000	-0.812	-0.497
h_1	1.9274 ± 0.10524	-0.812	1.000	0.119
h_2	-2.0701 ± 0.019888	-0.497	0.119	1.000

for δf^N discussed in Sec. II D 2. The rescaling parameter $\partial \log \Lambda^2 / \partial \log p^2$ evaluated at $p^2 = M^2$ is then included as a parameter in the fit, with errors propagated along with those of the other fit parameters in Tables II and III. The results of the fit using the OCS model are displayed in Fig. 8 for various PDFs as ratios to the central CJ15 PDFs (computed using the off-shell parametrization (15) and the AV18 deuteron wave function). For most of the PDFs the effects of using the more restrictive OCS model are relatively small and generally within the $\Delta\chi^2 = 1$ bands for all wave function models. The largest effects are for the d-quark distribution, where the results with the WJC-1 wave function show greater deviation at intermediate and large x values, suggesting that the hard tail of its momentum distribution may be more difficult to accommodate also
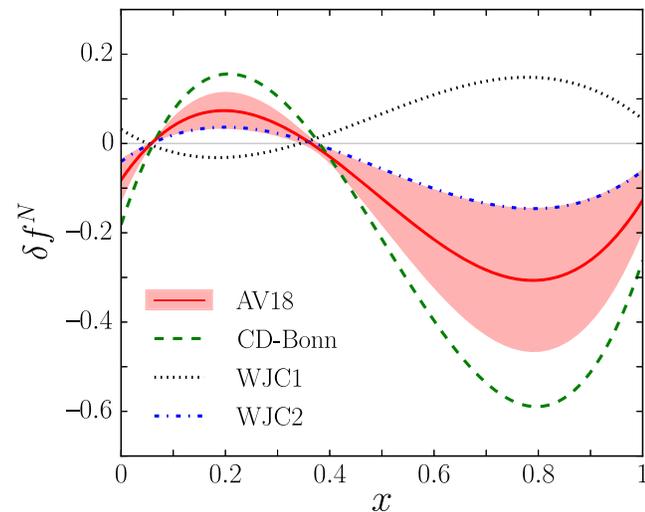

FIG. 7. Fitted nucleon off-shell correction δf^N for the parametrization in Eq. (15), using the AV18 (solid red curve with 90% C.L. uncertainty band), CD-Bonn (dashed green curve), WJC-1 (dotted black curve) and WJC-2 (dot-dashed blue curve) wave functions.

within the OCS model. The overall χ^2 values for all wave functions are similar to those of the main CJ15 fit, with differences in χ^2/datum appearing only in the third decimal place.

We should note, however, that the off-shell correction term δf^N, or even the off-shell PDF $\tilde{q}^N$ in Eq. (10), alone is nonphysical. Only the convolution of $\tilde{q}^N$ with the smearing function $f_{N/d}$ in Eq. (9) corresponds to the physical deuteron parton distribution (or structure function), and the two corrections (deuteron wave function and nucleon off-shell) must always be considered together. Since the off-shell correction is fitted, changes in deuteron wave function can in practice be compensated by a corresponding change in the off-shell parameters, to the extent allowed by the specific choice of wave function and off-shell parametrization.

This is clearly illustrated in Fig. 9, where the deuteron to nucleon F_2^d/F_2^N ratio is shown for the four different wave functions considered, and the three-parameter off-shell parametrization in Eq. (15). Remarkably, the structure function ratio is almost identical for the AV18, CD-Bonn and WJC-2 models. The slightly larger differences with the WJC-1 result reflecting the observations in Figs. 6–8 above, but even in this case the ratio is within the $\Delta\chi^2 = 1$ uncertainty band.

In addition to the important role played by nuclear corrections in F_2^d at large values of x, the effects of finite-Q^2 corrections are also significant, especially at low Q^2. In an earlier study [12], a nontrivial interplay was observed between the kinematic TMCs and the dynamical higher-twist corrections parametrized in Eq. (7). The impact of the finite-Q^2 corrections on the F_2^d/F_2^N ratio is illustrated in Fig. 10 for the CJ15 fit, for Q^2 between 2 and 100 GeV^2. The rise in the ratio at large x is fastest at the highest-Q^2 value and becomes less steep with decreasing Q^2. The general shape remains independent of the scale for $Q^2 \gtrsim 5$ GeV^2; however, a dramatic change occurs at $Q^2 \sim 2$ GeV^2, where F_2^d/F_2^N rises slowly until $x \approx 0.75$, before abruptly turning down for larger x. This behavior arises from the interplay between the target mass and higher-twist corrections to the free and bound nucleon structure functions, and the Q^2 dependent corrections to the smearing functions $f_{N/d}$ at finite values of Q^2.

For the standard TMC prescription adopted in this analysis, based on the operator product expansion [43], the fitted higher-twist coefficient function C_{HT} in Eq. (8) is plotted in Fig. 11, with the parameters given in Table III for the CJ15 fit. The coefficient displays the characteristic rise at large values of x observed in previous higher-twist extractions, and is almost completely independent of the deuteron wave function model over the entire range of x considered. For LO fits, the higher-twist function also absorbs part of the missing NLO contributions, resulting in
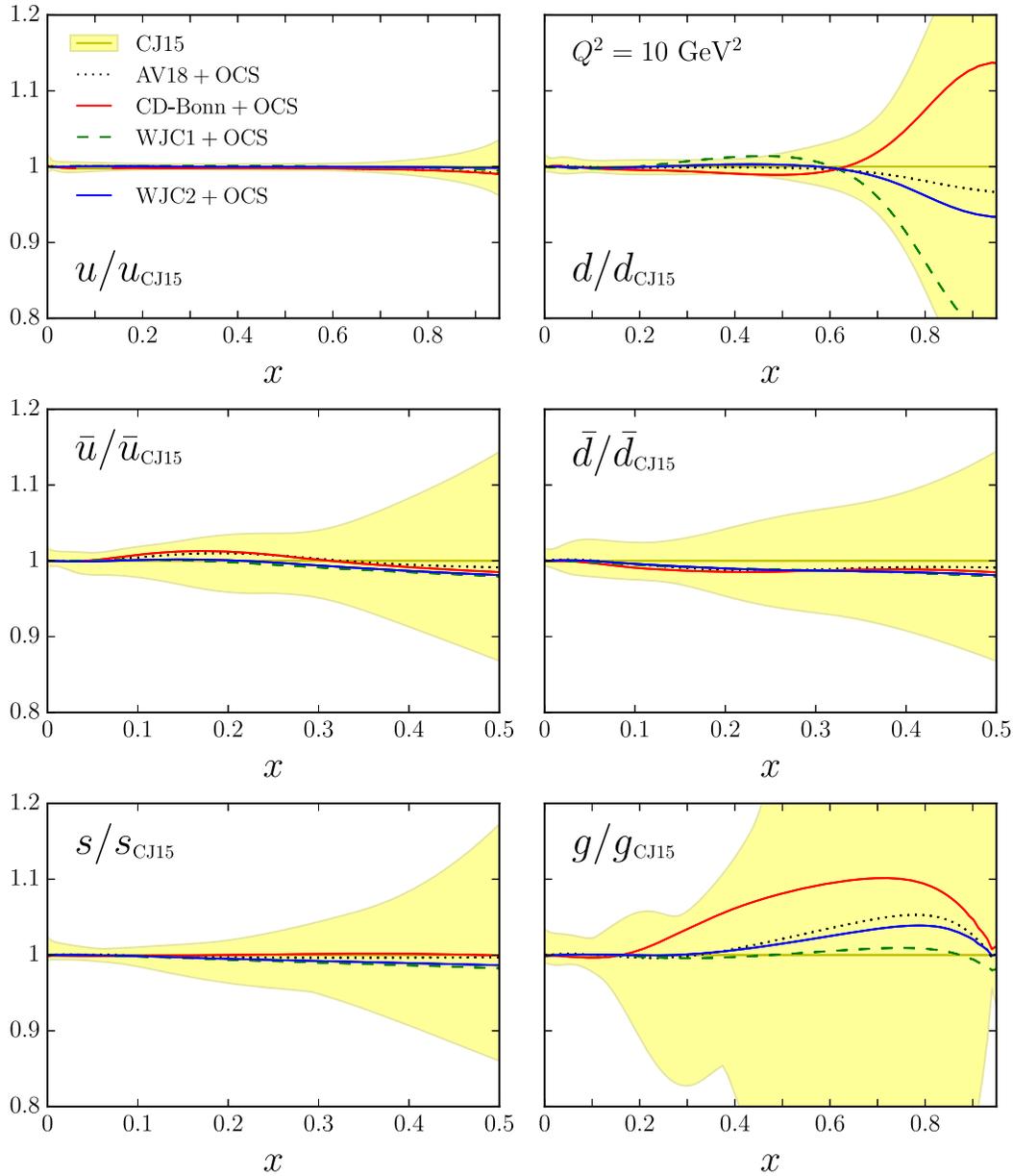
FIG. 8.   Ratio of PDFs computed using the off-shell covariant spectator (OCS) model and different deuteron wave functions to the CJ15 PDFs (which use the off-shell parametrization (15) and the AV18 deuteron wave function): OCS model with the AV18 wave function (black dotted curves), CD-Bonn (solid red curves), WJC-1 (dashed green curves), and WJC-2 (solid blue curves). The yellow band shows the 90% C.L. for the CJ15 fit.

higher values of the C_{HT} coefficient at large x, as was observed also in Refs. [57,105].

D. d/u ratio

The nuclear and finite-Q^2 corrections that manifest themselves in the F_2^d/F_2^N ratio as observed in Figs. 9 and 10 directly translate into modifying the behavior of the d/u PDF ratio at large x. Our previous analyses [12–14] have made detailed studies of the relationship between the size of the nuclear corrections in the deuteron and the shape and $x \to 1$ limit of d/u. For the CJ12 PDFs [14], three sets

of nuclear corrections were considered, corresponding to mild, medium and strong nuclear corrections, and referred to as "CJ12min", "CJ12mid" and "CJ12max," respectively. Each of these sets was consistent with the available data constraints and provided a convenient way to explore the nuclear effects on various observables.

Since our last analysis, the new data from the DØ Collaboration on charged lepton [17,18] and W boson asymmetries [19] that have become available have allowed significant new constraints to be placed on the d/u ratio at high x. The new DØ electron and muon asymmetry data,
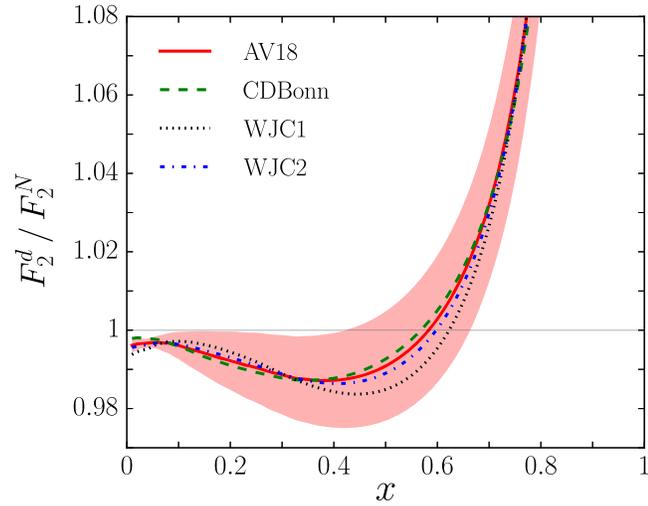
FIG. 9. Ratio of deuteron to isoscalar nucleon structure functions F_2^d/F_2^N for different deuteron wave function models at $Q^2 = 10$ GeV^2: AV18 (solid red curve with 90% C.L. uncertainty band), CD-Bonn (dashed green curve), WJC-1 (dotted black curve) and WJC-2 (dot-dashed blue curve).
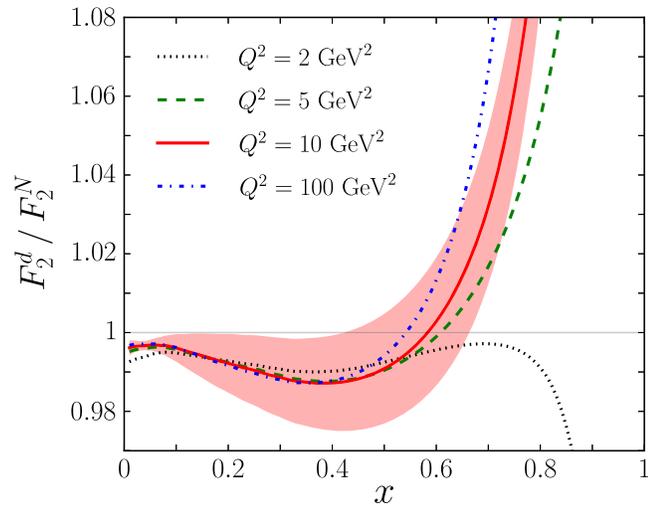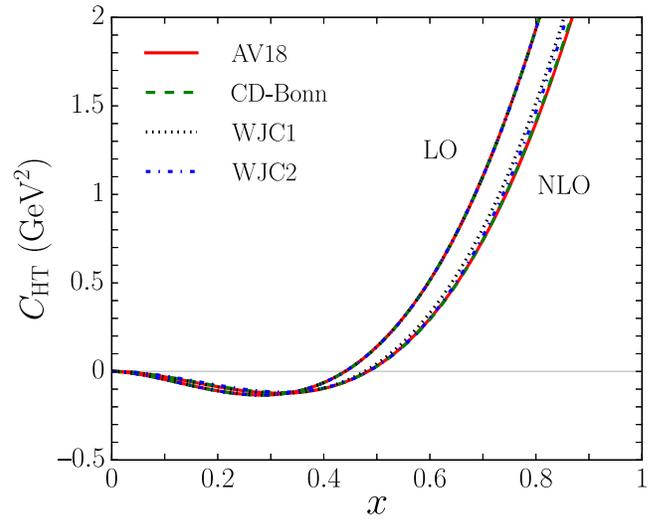

FIG. 11. Fitted higher twist function C_{HT} from Eq. (8), in units of GeV^2, for different deuteron wave function models. The higher twist term for the CJ15 NLO fit is compared with the corresponding term in the LO fit. The 90% C.L. uncertainty band is barely visible and is not shown here.
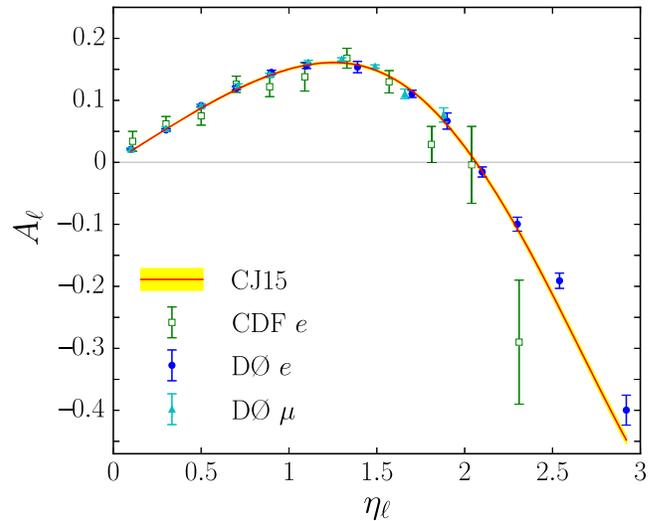

FIG. 10. Ratio of deuteron to isoscalar nucleon structure functions F_2^d/F_2^N computed from the CJ15 PDFs for different values of Q^2: 2 GeV^2 (dotted black curve), 5 GeV^2 (dashed green curve), 10 GeV^2 (solid red curve with 90% C.L. uncertainty band) and 100 GeV^2 (dot-dashed blue curve).

FIG. 12. Lepton charge asymmetry A_ℓ from $p\bar{p} \to WX \to \ell\nu X$ as a function of the lepton pseudorapidity η_ℓ from CDF electron (green open squares) [88], DØ electron (blue circles) [18] and DØ muon (cyan triangles) [17] data compared with the CJ15 fit with 90% C.L. uncertainty (yellow band).

together with earlier data from CDF [88], are displayed in Fig. 12 as a function of the lepton pseudorapidity η_l and compared with the CJ15 fit. The extracted W boson asymmetries, which are more directly related to the shape of the PDFs and are not limited in their x reach by the lepton decay vertex smearing, are shown in Fig. 13 as a function of the W boson rapidity y_W. The statistical errors on the DØ data in particular are extremely small and place strong constraints on the fit. The earlier CDF electron and

W data have larger errors and have more limited constraining power. Compared with the range of nuclear corrections in CJ12, the asymmetry data, and especially the new results from DØ, strongly favor smaller nuclear corrections at large x, closer to those in the CJ12min set.

The stronger constraints from the lepton and W charge asymmetry data lead to a significant reduction in the uncertainties on the d/u ratio, particularly at large values
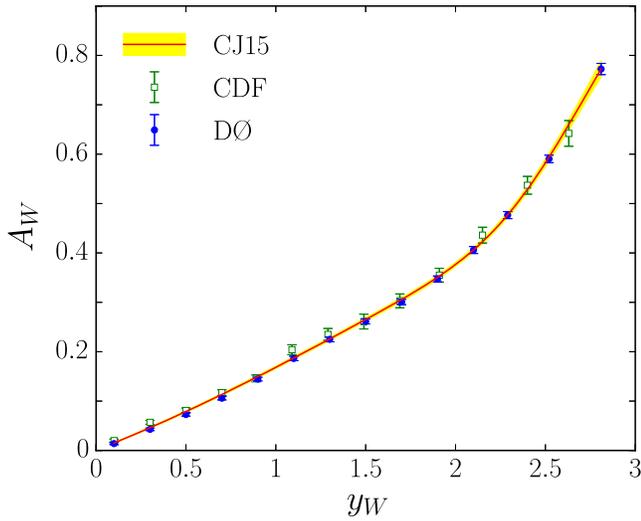
FIG. 13. W boson charge asymmetry A_W from $p\bar{p} \to WX$ as a function of the W boson rapidity y_W for CDF (green open squares) [89] and DØ (blue circles) [19] data compared with the CJ15 fit with 90% C.L. uncertainty (yellow band).

of x. This is illustrated in Fig. 14, which demonstrates the shrinking of the d/u uncertainty bands (which are shown here and in the remainder of this section at the 90% C.L.) with the successive addition of various data sets. Compared with the fit to DIS only data, in which the d/u ratio has very large uncertainties beyond $x \approx 0.4$, the addition of the lepton asymmetries leads to a reduction in d/u of more than a factor of two at $x \lesssim 0.4$, with more limited impact at
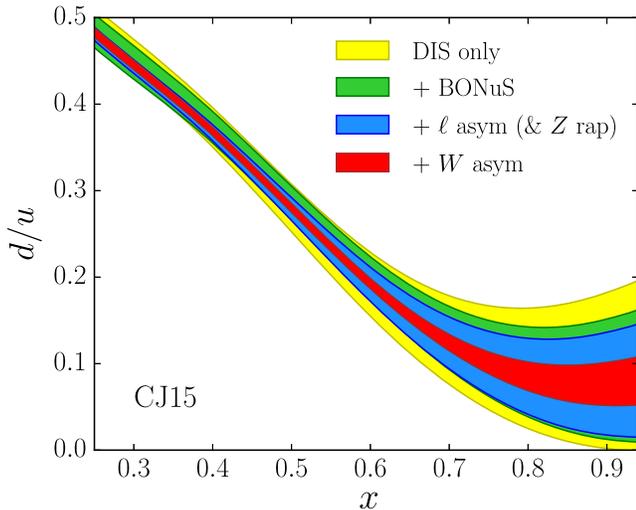

FIG. 14.   Impact of various data sets on the d/u ratio at $Q^2 = 10$ GeV^2. The 90% C.L. uncertainty band is largest for the DIS only data (yellow band), and decreases with the successive addition of Jefferson Lab BONuS F_2^n/F_2^d [21] data (green band), lepton asymmetry [17,18,88] (and Z rapidity [90,91]) data (blue band), and W boson asymmetry data [19,89] (red band).

higher-x values due to the PDF smearing caused by the lepton decay vertex. (Addition of Z boson rapidity data [90,91] has only modest impact on d/u.) Subsequent inclusion of the W asymmetries leads to a further halving of the uncertainty at $x \approx 0.6$–0.8, while having minimal effect on the errors at $x \lesssim 0.4$.

In fact, independent of the charge asymmetry data, a significant reduction in the d/u uncertainty at intermediate x values is already provided by the Jefferson Lab BONuS data on F_2^n/F_2^d [20,21]. While the BONuS data have little or no effect at $x \lesssim 0.3$, the reduction in the d/u error at $x \sim 0.5$–0.6 is almost as large as that from the lepton asymmetries. (The BONuS data have a slight preference for stronger nuclear corrections, in contrast to the lepton asymmetry data, although the tension is not significant.) Using all the available data from DIS and W boson production, the central value of the extrapolated d/u ratio at $x = 1$ is ≈ 0.1 at the input scale Q_0^2. The nuclear model dependence of the central values of the $x \to 1$ limit of d/u is relatively weak, ranging from 0.08 for the WJC-1 wave function to 0.12 for the CD-Bonn model. For our best fit, we obtain the extrapolated value,

$$d/u \xrightarrow[x \to 1]{} 0.09 \pm 0.03, \qquad (16)$$

at the 90% C.L., which represents a factor ≈ 2 reduction in the central value compared with the CJ12 result [14].

While the new charge asymmetry and BONuS F_2^n/F_2^d measurements provide important constraints on the d/u ratio, the existing inclusive deuteron DIS data still play an important role in global analyses, as does the proper treatment of the nuclear corrections. If one were to fit F_2^d data without accounting for nuclear effects (assuming $F_2^d = F_2^p + F_2^n$), the resulting d/u ratio would be strongly overestimated beyond $x = 0.6$, where the F_2^d/F_2^N ratio begins to deviate significantly from unity (see Fig. 9). This is illustrated in Fig. 15, where the CJ15 d/u ratio is compared with the fit without nuclear corrections. This behavior can be understood from the shape of the F_2^d/F_2^N ratio Fig. 9 at large x, where the effect of the nuclear corrections is to increase the ratio above unity for $x \gtrsim 0.6$. Since F_2^d and F_2^p are fixed inputs, a larger F_2^d/F_2^N is generated by a smaller neutron F_2^n and hence a smaller d/u ratio. For example, the effect of the nuclear corrections is to shift the d/u ratio at $x = 0.8$ from the range ≈ 0.1–0.3 to ≈ 0–0.2 once the smearing and off-shell effects are included. Removing the deuterium data altogether increases the overall uncertainty band for $x \gtrsim 0.7$. The deuteron data also reduce the d/u uncertainties slightly at smaller values of $x \lesssim 0.2$ (see below).

Effects on large-x PDFs from nuclear corrections have also been investigated by several other groups in recent years [6,10,80,99,106] and it is instructive to compare the CJ15 results on the d/u ratio with those analyses.
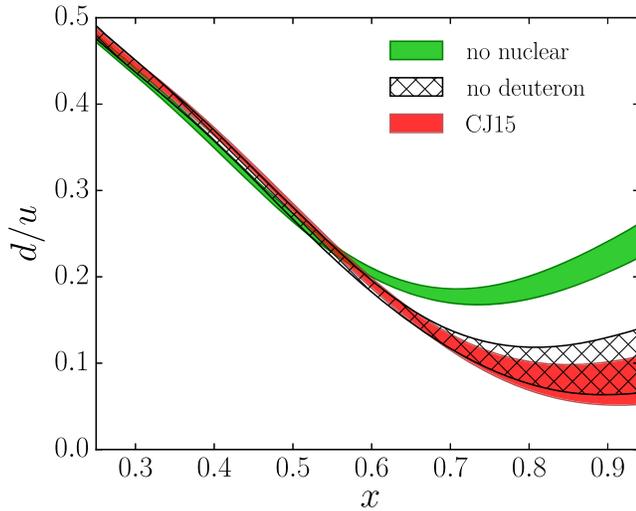
FIG. 15. Impact on the CJ15 d/u ratio at $Q^2 = 10 \text{ GeV}^2$ (red band) of removing the deuterium nuclear corrections (green band), and omitting the deuterium data (cross-hatched band).
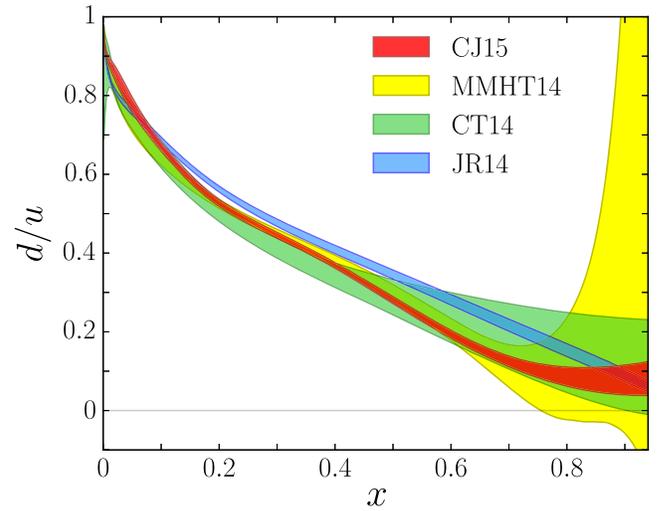

FIG. 16. Comparison of the d/u ratio at $Q^2 = 10 \text{ GeV}^2$ for different PDF parametrizations: CJ15 (red band), MMHT14 [6] (yellow band, 68% C.L.), CT14 [7] (green band), and JR14 [10] (blue band, scaled by a factor 1.645 for the 90% C.L.).

The MMHT14 fit [6] uses a purely phenomenological, Q^2-independent nuclear correction for the combined effects of nuclear smearing and off-shell corrections, in contrast to our approach in which the (poorly understood) off-shell correction is fitted, but the (better known) deuteron wave function correction is computed, and finite-Q^2 effects are taken into account. Interestingly, the phenomenological MMHT14 F_2^d/F_2^N ratio has a qualitatively similar shape to that found in our more microscopic estimate, which offers an important cross check of our formalism. For $x \lesssim 0.7$, the MMHT14 d/u uncertainty is comparable to that in CJ15, although for $x \gtrsim 0.8$ the uncertainty diverges rapidly due to the adoption of a stiffer d-quark parametrization, which only allows the d/u ratio to approach zero or infinity as $x \to 1$.

The JR14 analysis [10] uses similar smearing functions to those used in our fit, but does not include nucleon off-shell corrections. Furthermore, it uses the $\Delta\chi^2 = 1$ criterion for the 1σ C.L., based on statistical considerations alone, introducing additional systematic uncertainties through the dependence of the fit on the input scale. The resulting uncertainty on d/u is larger than that in CJ15 in the intermediate-x region, which may reflect the absence of the recent W and lepton asymmetry data in the JR14 fit. The range of d/u values extrapolated to $x = 1$ is similar to the CJ15 band within errors, although the form of the JR14 parametrization forces $d/u \to 0$ at $x = 1$.

The CJ15 uncertainty band in Fig. 16 is also similar to that found in the CT14 global analysis [7], which does not apply any nuclear corrections to deuterium data, on the basis of the somewhat higher W^2 cuts utilized. The CT14 analysis uses a parametrization based on Bernstein polynomials multiplying a common factor $x^{a_1}(1-x)^{a_2}$, and fixes the exponents a_2 to be the same for the u- and d-quark

PDFs, thereby allowing finite values of the d/u ratio in the $x \to 1$ limit. The results of the two analyses largely overlap over much of the x range, with the CT14 distributions being slightly above the CJ15 error band at $x \gtrsim 0.6$. This is reminiscent of the higher d/u ratio observed in Fig. 15 when the nuclear corrections are switched off.

Finally, in Fig. 17 we show the d/u uncertainty from the CJ15 fit compared with the uncertainties obtained in fits excluding DIS deuteron or W asymmetry data. The W asymmetry data, which are statistically dominated by the
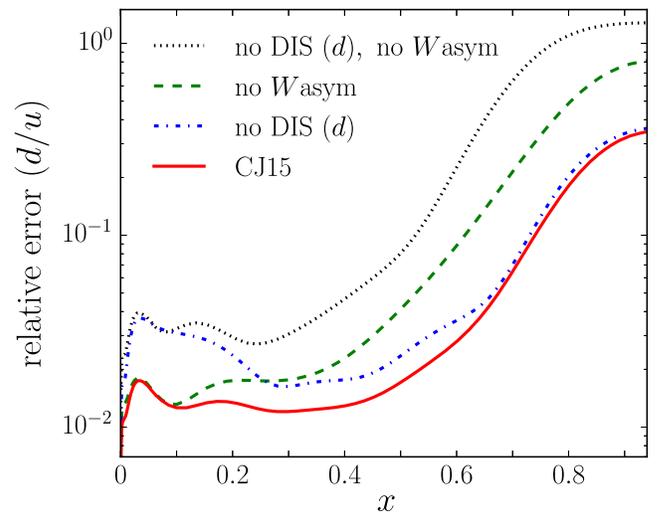

FIG. 17. Relative error on the d/u PDF ratio versus x at $Q^2 = 10 \text{ GeV}^2$ from the CJ15 fit (90% C.L., solid red curve) compared with the uncertainties obtained in fits excluding deuteron DIS data (dot-dashed blue curve) or W asymmetry data (dashed green curve), as well as excluding both (dotted black curve).

DØ results, provide the main constraint on the d/u ratio at $x \gtrsim 0.3$. At $x \lesssim 0.3$, where the statistical power of the reconstructed W asymmetry data becomes limited, the global deuteron DIS data play a vital role in reducing the uncertainty in the d/u ratio by more than 50%. At $x \gtrsim 0.6$, the statistical power of the DIS data is utilized instead to fit the off-shell function δf^N. The combination of these two observables provides a good illustration of the complementarity of different data sets in global fits in constraining PDFs over extended regions of x.

V. CONCLUSION

We have presented here results of the CJ15 global NLO analysis of parton distributions, taking into account the latest developments in theory and the availability of new data. Focusing particularly, but not exclusively, on the large-x region, the new analysis features a more comprehensive treatment of nuclear corrections to deuterium data, as well as a more flexible parametrization of the SU(2) light antiquark asymmetry, and an improved treatment of heavy quarks. In contrast to the earlier CJ12 fit [14], which used physically motivated models for the nucleon off-shell corrections, the present analysis allows the magnitude and shape of the off-shell effects to be phenomenologically constrained directly from data.

Along with the expanded set of proton and deuteron DIS data afforded by our less restrictive kinematic cuts $Q^2 > (1.3 \text{ GeV})^2$ and $W^2 > 3 \text{ GeV}^2$, we also include new results from the BONuS experiment at Jefferson Lab [20,21], which provide the first determination of the neutron structure function essentially free of nuclear correction uncertainties. The greatest impact on the fits, however, comes from the new DØ W asymmetry data at large rapidity [19], which because of their high precision and kinematic reach are able to place significant constraints on PDFs at high x. In particular, while the previous CJ12 analysis provided three sets of PDFs corresponding to a range of different deuterium and off-shell models, the new W asymmetry data strongly favor models with smaller nuclear corrections, closer to the "CJ12min" PDF set [14]. Within the parametrization of the nucleon off-shell corrections adopted here, our analysis has a slight preference for deuteron wave functions with softer momentum distributions, but essentially indistinguishable fits can be obtained with each of the deuteron models considered.

Our approach to the nuclear corrections is similar in spirit to the phenomenological analysis of Ref. [66], which makes use of DIS data on a wide range of nuclear targets and finds the ratio F_2^d/F_2^N to have a universal shape similar to that for F_2^A/F_2^d for heavy nuclei. From the proton and deuterium data alone, however, we find no evidence for an enhancement of F_2^d/F_2^N in the vicinity of $x \approx 0.1$. The only way to definitively resolve this question may be with data on the free neutron structure function that are not subject to

assumptions about nuclear corrections in deuterium. The phenomenological approach of fitting the nuclear effects directly was also utilized in Refs. [6,80], who parametrized the entire nuclear correction by a function that mimics both the effects of the smearing and the nucleon off-shell correction. Since the nuclear physics of the deuteron at long distances is relatively well understood, our philosophy is to include in the theoretical description the effects that can be computed reliably, and parametrize those that are more strongly model dependent.

As anticipated in Refs. [14,23] and elaborated in Ref. [104], the new precision measurements of observables that are sensitive to the d-quark PDF, but less sensitive to nuclear corrections, are seen to play an important role in allowing global QCD fits to constrain models of nuclear corrections in the deuteron. In particular, a simultaneous fit of the new W charge asymmetries [19] and the SLAC deuteron DIS structure functions [82] is only possible when nuclear corrections are taken into account. The interplay of these two data sets within the CJ15 fit has provided the first determination of nucleon off-shell effects in quark distributions in the deuteron within a global QCD context. At the same time, the d/u ratio has seen a significant reduction in its uncertainty at $x \gtrsim 0.5$, with an extrapolated central value ≈ 0.1 at $x \to 1$, or about half of that found in the CJ12 fit [14]. As discussed in Refs. [107,108], a precise determination of the d-quark PDF at large x is vital for searches for physics beyond the standard model at the LHC at the edges of kinematics, such as at large rapidities in heavy weak-boson production or, more generally, in large invariant mass observables.

The uncertainty in the d/u ratio is expected to be further reduced once new data from experiments at the energy-upgraded Jefferson Lab facility become available [101–103], that will probe PDFs up to $x \sim 0.85$ at DIS kinematics. The first of these, involving the simultaneous measurement of inclusive DIS cross section from ^{3}He and ^{3}H [101], in which the nuclear corrections are expected to mostly cancel [109–112], is scheduled to begin data taking in Fall 2016. The current analysis provides a timely benchmark against which the upcoming experimental results can be calibrated.

[1] P. Jimenez-Delgado, W. Melnitchouk, and J. F. Owens, J. Phys. G **40**, 093102 (2013).

[2] J. Blümlein, Prog. Part. Nucl. Phys. **69**, 28 (2013).

[3] S. Forte and G. Watt, Annu. Rev. Nucl. Part. Sci. **63**, 291 (2013).

[4] A. M. Cooper-Sarkar, Proc. Sci., DIS2015 (**2015**) 005, arXiv:1507.03849.

[5] M. E. Christy and W. Melnitchouk, J. Phys. Conf. Ser. **299**, 012004 (2011).

[6] L. A. Harland-Lang, A. D. Martin, P. Motylinski, and R. S. Thorne, Eur. Phys. J. C **75**, 204 (2015).

[7] S. Dulat, T.-J. Hou, J. Gao, M. Guzzi, J. Huston, P. Nadolsky, J. Pumplin, C. Schmidt, D. Stump, and C.-P. Yuan, Phys. Rev. D **93**, 033006 (2016).

[8] R. D. Ball et al., J. High Energy Phys. 04 (2015) 040.

[9] V. Radescu, in *Proceedings of 35th International Conference of High Energy Physics (ICHEP2010)*, Paris, France (2010), arXiv:1308.0374.

[10] P. Jimenez-Delgado and E. Reya, Phys. Rev. D **89**, 074049 (2014).

[11] S. Alekhin, J. Blüemlein, S. Moch, and R. Placakyte, arXiv:1508.07923.

[12] A. Accardi, M. E. Christy, C. E. Keppel, P. Monaghan, W. Melnitchouk, J. G. Morfin, and J. F. Owens, Phys. Rev. D **81**, 034016 (2010).

[13] A. Accardi, W. Melnitchouk, J. F. Owens, M. E. Christy, C. E. Keppel, L. Zhu, and J. G. Morfin, Phys. Rev. D **84**, 014008 (2011).

[14] J. F. Owens, A. Accardi, and W. Melnitchouk, Phys. Rev. D **87**, 094012 (2013).

[15] The CTEQ-Jefferson Lab (CJ) Collaboration, http://www.jlab.org/cj.

[16] W. Melnitchouk and A. W. Thomas, Phys. Lett. B **377**, 11 (1996).

[17] V. M. Abazov et al., Phys. Rev. D **88**, 091102 (2013).

[18] V. M. Abazov et al., Phys. Rev. D **91**, 032007 (2015).

[19] V. M. Abazov et al., Phys. Rev. Lett. **112**, 151803 (2014); **114**, 049901 (2015).

[20] N. Baillie et al., Phys. Rev. Lett. **108**, 142001 (2012).

[21] S. Tkachenko et al., Phys. Rev. C **89**, 045206 (2014).

[22] M. Krämer, F. I. Olness, and D. E. Soper, Phys. Rev. D **62**, 096007 (2000).

[23] A. Accardi, Mod. Phys. Lett. A **28**, 1330032 (2013).

[24] G. R. Farrar and D. R. Jackson, Phys. Rev. Lett. **35**, 1416 (1975).

[25] F. E. Close, Phys. Lett. **43B**, 422 (1973).

[26] F. E. Close and W. Melnitchouk, Phys. Rev. C **68**, 035210 (2003).

[27] R. J. Holt and C. D. Roberts, Rev. Mod. Phys. **82**, 2991 (2010).

[28] C. D. Roberts, R. J. Holt, and S. M. Schmidt, Phys. Lett. B **727**, 249 (2013).

[29] E. A. Hawker et al., Phys. Rev. Lett. **80**, 3715 (1998); J. Webb, Ph.D. Thesis, New Mexico State University, 2002, arXiv:hep-ex/0301031.

[30] R. S. Towell et al., Phys. Rev. D **64**, 052002 (2001).

[31] Fermilab E906 experiment (SeaQuest), Drell-Yan measurements of nucleon and nuclear structure with the Fermilab main injector, http://www.phy.anl.gov/mep/SeaQuest/index.html.

[32] A. Accardi, F. Arleo, W. K. Brooks, D. D'Enterria, and V. Muccifora, Riv. Nuovo Cimento **32**, 439 (2010).

[33] A. Majumder and M. van Leeuwen, Prog. Part. Nucl. Phys. **66**, 41 (2011).

[34] K. J. Eskola, H. Paukkunen, and C. A. Salgado, J. High Energy Phys. 04 (2009) 065.

[35] D. de Florian, R. Sassot, P. Zurita, and M. Stratmann, Phys. Rev. D **85**, 074028 (2012).

[36] K. Kovarik et al., Phys. Rev. D **93**, 085037 (2016).

[37] G. Aad et al., Phys. Rev. Lett. **109**, 012001 (2012).

[38] S. Alekhin, J. Blümlein, L. Caminadac, K. Lipka, K. Lohwasser, S. Moch, R. Petti, and R. Placakyte, Phys. Rev. D **91**, 094002 (2015).

[39] S. Catani, D. de Florian, G. Rodrigo, and W. Vogelsang, Phys. Rev. Lett. **93**, 152003 (2004).

[40] A. I. Signal and A. W. Thomas, Phys. Lett. B **191**, 205 (1987).

[41] G. P. Zeller et al., Phys. Rev. D **65**, 111103 (2002); **67**, 119902 (2003).

[42] F. I. Olness and W.-K. Tung, Nucl. Phys. **B308**, 813 (1988); M. A. Aivazis, F. I. Olness, and W.-K. Tung, Phys. Rev. D **50**, 3085 (1994); M. A. Aivazis, J. C. Collins, F. I. Olness, and W.-K. Tung, Phys. Rev. D **50**, 3102 (1994).

[43] H. Georgi and H. D. Politzer, Phys. Rev. D **14**, 1829 (1976).

[44] I. Schienbein et al., J. Phys. G **35**, 053101 (2008).

[45] L. T. Brady, A. Accardi, T. J. Hobbs, and W. Melnitchouk, Phys. Rev. D **84**, 074008 (2011); **85**, 039902 (2012).

[46] O. W. Greenberg and D. Bhaumik, Phys. Rev. D **4**, 2048 (1971).

[47] O. Nachtmann, Nucl. Phys. **B63**, 237 (1973).

[48] R. K. Ellis, R. Petronzio, and G. Parisi, Phys. Lett. **64B**, 97 (1976).

[49] A. Accardi, T. Hobbs, and W. Melnitchouk, J. High Energy Phys. 11 (2009) 084.

[50] J. V. Guerrero, J. J. Ethier, A. Accardi, S. W. Casper, and W. Melnitchouk, J. High Energy Phys. 09 (2015) 169.

[51] M. A. G. Aivazis, F. I. Olness, and W. K. Tung, Phys. Rev. D **50**, 3085 (1994).

[52] S. Kretzer and M. H. Reno, Phys. Rev. D **66**, 113007 (2002).

[53] A. Accardi and J.-W. Qiu, J. High Energy Phys. 07 (2008) 090.

[54] F. M. Steffens, M. D. Brown, W. Melnitchouk, and S. Sanches, Phys. Rev. C **86**, 065208 (2012).

[55] M. Virchaux and A. Milsztajn, Phys. Lett. B **274**, 221 (1992).

[56] S. I. Alekhin, S. A. Kulagin, and S. Liuti, Phys. Rev. D **69**, 114009 (2004).

[57] J. Blümlein and H. Böttcher, Phys. Lett. B **662**, 336 (2008).

[58] J. Blümlein, Prog. Part. Nucl. Phys. **69**, 28 (2013).

[59] B. Badelek and J. Kwiecinski, Nucl. Phys. **B370**, 278 (1992).

[60] W. Melnitchouk and A. W. Thomas, Phys. Rev. D **47**, 3783 (1993).

[61] L. P. Kaptari and A. Y. Umnikov, Phys. Lett. B **272**, 359 (1991).

[62] W. Melnitchouk, A. W. Schreiber, and A. W. Thomas, Phys. Rev. D **49**, 1183 (1994).

[63] S. A. Kulagin, G. Piller, and W. Weise, Phys. Rev. C **50,** 1154 (1994).

[64] P. J. Ehlers, A. Accardi, L. T. Brady, and W. Melnitchouk, Phys. Rev. D **90,** 014010 (2014).

[65] S. A. Kulagin, W. Melnitchouk, G. Piller, and W. Weise, Phys. Rev. C **52,** 932 (1995).

[66] S. A. Kulagin and R. Petti, Nucl. Phys. **A765,** 126 (2006).

[67] Y. Kahn, W. Melnitchouk, and S. A. Kulagin, Phys. Rev. C **79,** 035205 (2009).

[68] R. B. Wiringa, V. G. J. Stoks, and R. Schiavilla, Phys. Rev. C **51,** 38 (1995).

[69] R. Machleidt, Phys. Rev. C **63,** 024001 (2001).

[70] F. Gross and A. Stadler, Phys. Rev. C **78,** 014005 (2008); **82,** 034004 (2010).

[71] J. Arrington, F. Coester, R. J. Holt, and T.-S. H. Lee, J. Phys. G **36,** 025005 (2009).

[72] J. Arrington, J. G. Rubin, and W. Melnitchouk, Phys. Rev. Lett. **108,** 252001 (2012).

[73] F. Gross and S. Liuti, Phys. Rev. C **45,** 1374 (1992).

[74] W. Melnitchouk, A. W. Schreiber, and A. W. Thomas, Phys. Lett. B **335,** 11 (1994).

[75] W. Melnitchouk, M. Sargsian, and M. Strikman, Z. Phys. A **359,** 99 (1997).

[76] H. Mineo, W. Bentz, N. Ishii, A. W. Thomas, and K. Yazaki, Nucl. Phys. **A735,** 482 (2004).

[77] I. C. Cloet, W. Bentz, and A. W. Thomas, Phys. Lett. B **642,** 210 (2006).

[78] J. J. Aubert et al., Phys. Lett. **123B,** 275 (1983).

[79] D. F. Geesaman, K. Saito, and A. W. Thomas, Annu. Rev. Nucl. Part. Sci. **45,** 337 (1995).

[80] A. D. Martin, A. J. Th. M. Mathijssen, W. J. Stirling, R. S. Thorne, B. J. A. Watt, and G. Watt, Eur. Phys. J. C **73,** 2318 (2013).

[81] A. C. Benvenuti et al., Phys. Lett. B **223,** 485 (1989); **236,** 592 (1989).

[82] L. W. Whitlow, E. M. Riordan, S. Dasu, S. Rock, and A. Bodek, Phys. Lett. B **282,** 475 (1992).

[83] M. Arneodo et al., Nucl. Phys. **B483,** 3 (1997).

[84] M. Arneodo et al., Nucl. Phys. **B487,** 3 (1997).

[85] H. Abramowicz et al., Eur. Phys. J. C **75,** 580 (2015).

[86] A. Airapetian et al., J. High Energy Phys. 05 (2011) 126.

[87] S. P. Malace et al., Phys. Rev. C **80,** 035207 (2009).

[88] D. Acosta et al., Phys. Rev. D **71,** 051104(R) (2005).

[89] T. Aaltonen et al., Phys. Rev. Lett. **102,** 181801 (2009).

[90] T. Aaltonen et al., Phys. Lett. B **692,** 232 (2010).

[91] V. M. Abazov et al., Phys. Rev. D **76,** 012003 (2007).

[92] T. Aaltonen et al., Phys. Rev. D **78,** 052006 (2008).

[93] V. M. Abazov et al., Phys. Rev. Lett. **101,** 062001 (2008); B. Abbott et al., Phys. Rev. Lett. **86,** 1707 (2001).

[94] V. M. Abazov et al., Phys. Lett. B **666,** 435 (2008).

[95] S. Alekhin, K. Melnikov, and F. Petriello, Phys. Rev. D **74,** 054033 (2006).

[96] G. Moreno et al., Phys. Rev. D **43,** 2815 (1991).

[97] P. Jimenez-Delgado, T. J. Hobbs, J. T. Londergan, and W. Melnitchouk, Phys. Rev. Lett. **114,** 082002 (2015).

[98] K. A. Olive et al., Chin. Phys. C **38,** 090001 (2014).

[99] S. Alekhin, J. Blümlein, and S.-O. Moch, Phys. Rev. D **86,** 054009 (2012).

[100] L. A. Harland-Lang, A. D. Martin, P. Motylinski, and R. S. Thorne, Eur. Phys. J. C **76,** 186 (2016).

[101] Jefferson Lab Experiment C12-10-103 (MARATHON), G. G. Petratos, J. Gomez, R. J. Holt, and R. D. Ransome, spokespersons.

[102] Jefferson Lab Experiment E12-10-102 (BONUS12), S. Bültmann, M. E. Christy, H. Fenker, K. Griffioen, C. E. Keppel, S. Kuhn, and W. Melnitchouk, spokespersons.

[103] Jefferson Lab Experiment E12-10-007 (SoLID), P. Souder, spokesperson.

[104] A. Accardi, Proc. Sci., DIS2015 (**2015**) 001, arXiv:1602.02035.

[105] A. D. Martin, R. G. Roberts, W. J. Stirling, and R. S. Thorne, Eur. Phys. J. C **35,** 325 (2004).

[106] S. Alekhin, J. Blümlein, S. Klein, and S.-O. Moch, Phys. Rev. D **81,** 014032 (2010).

[107] L. T. Brady, A. Accardi, W. Melnitchouk, and J. F. Owens, J. High Energy Phys. 06 (2012) 019.

[108] A. Accardi et al., arXiv:1603.08906.

[109] I. R. Afnan, F. Bissey, J. Gomez, A. T. Katramatou, W. Melnitchouk, G. G. Petratos, and A. W. Thomas, Phys. Lett. B **493,** 36 (2000);

[110] I. R. Afnan, F. Bissey, J. Gomez, A. T. Katramatou, S. Liuti, W. Melnitchouk, G. G. Petratos, and A. W. Thomas Phys. Rev. C **68,** 035201 (2003).

[111] E. Pace, G. Salme, S. Scopetta, and A. Kievsky, Phys. Rev. C **64,** 055203 (2001).

[112] M. M. Sargsian, S. Simula, and M. I. Strikman, Phys. Rev. C **66,** 024001 (2002).